Title:

Mutational biases promote neutral increases in the complexity of protein interaction networks following gene duplication

Authors:

Angel F. Cisneros[1,2,3,4], Lou Nielly-Thibault[2,3,4,5], Saurav Mallik[6], Emmanuel D. Levy[6], Christian R. Landry[1,2,3,4,5]

Affiliations:

[1]Département de biochimie, de microbiologie et de bio-informatique, Faculté des sciences et de génie, Université Laval, G1V 0A6, Québec, Canada
[2]Institut de biologie intégrative et des systèmes, Université Laval, G1V 0A6, Québec, Canada
[3]PROTEO, Le regroupement québécois de recherche sur la fonction, l'ingénierie et les applications des protéines, Université Laval, G1V 0A6, Québec, Canada
[4]Centre de recherche sur les données massives, Université Laval, G1V 0A6, Québec, Canada
[5]Département de biologie, Faculté des sciences et de génie, Université Laval, G1V 0A6, Québec, Canada
[6]Department of Chemical and Structural Biology, Weizmann Institute of Science, 7610001, Rehovot, Israel

Correspondance:
Tel: +1 418 656 3954; E-mail: christian.landry@bio.ulaval.ca

Abstract

Biological systems can gain complexity over time. While some of these transitions are likely driven by natural selection, the extent to which they occur without providing an adaptive benefit is unknown. At the molecular level, one example is heteromeric complexes replacing homomeric ones following gene duplication. Here, we build a biophysical model and simulate the evolution of homodimers and heterodimers following gene duplication using distributions of mutational effects inferred from available protein structures. We keep the specific activity of each dimer identical, so their concentrations drift neutrally without new functions. We show that for more than 60% of tested dimer structures, the relative concentration of the heteromer increases over time due to mutational biases that favor the heterodimer. However, allowing mutational effects on synthesis rates and differences in the specific activity of homo- and heterodimers can limit or reverse the observed bias toward heterodimers. Our results show that the accumulation of more complex protein quaternary structures is likely under neutral evolution, and that natural selection would be needed to reverse this tendency.

Keywords

Gene duplication / mutational biases / neutral evolution / protein biophysics / protein interaction networks

2

Introduction

Gene duplication is a potent mechanism for the generation of novel molecular and phenotypic traits (Conant & Wolfe, 2008; Kuzmin *et al*, 2022). Duplication introduces an additional copy of a gene, which may allow sister copies to accumulate mutations that would not have been accessible before. The long-term maintenance of the duplicates could depend on one or both evolving new functions (Deng *et al*, 2010; Bridgham *et al*, 2008). Alternatively, the two copies could split the functions of the ancestral protein (Force *et al*, 1999; Lynch & Conery, 2000; He & Zhang, 2005; Baker *et al*, 2013). Under this model, the two copies show partial degeneration of their ancestral function and complement each other in accomplishing it. In this context, cellular biochemical or genetic networks become more complex (i.e. they have more parts and interactions) without net functional or fitness gain.

One context in which this increase in complexity takes place is the assembly of protein complexes. Following the duplication, two paralogous genes encode the product of the ancestral gene. In the case of the duplication of a gene encoding a homomeric protein complex (self-interacting protein), the paralogous proteins might assemble in a mixture of states (Pereira-Leal *et al*, 2007): two homodimers and a heterodimer in the case of dimers, with further combinatorial complexity depending on the number of subunits in the ancestral homomer. In this work, we will focus on homodimers because they are the most frequent type of homomers in proteomes. Indeed, homodimers amount to almost 66% of homomers and no other multimeric assembly exceeds 15% of homomers, with some variation depending on the species (Lynch, 2012, 2013; Levy & Teichmann, 2013; Schweke *et al*, 2023). An important consideration is that heteromers directly become the state with the highest concentration right after the duplication, and the energetic barrier needed for selective homomerization increases with the number of subunits (Hochberg *et al*, 2018). For example, the duplication of an ancestral homodimer would lead to 50% heterodimers and 25% of each homodimer at binding equilibrium if all their parameters are the same (synthesis rates, folding energies, binding affinities, etc.). As such, heteromers are expected to assume a significant proportion of the functional contributions directly after the duplication.

Given the prevalence of homomers and the significant role of gene duplications in evolution, it follows that heteromers composed of paralogous proteins constitute a substantial portion of the complexes within protein interaction networks. Indeed, these heteromeric interactions have been shown to be retained in more than 30% of paralogs in several species and are especially prevalent for duplicates with higher sequence identity (Marchant *et al*, 2019; Mallik & Tawfik, 2020). Interestingly, in some of these cases, the heteromer becomes the only active complex (Wang *et al*, 2006; Boncoeur *et al*, 2012) or diverges functionally (Bridgham *et al*, 2008; Baker *et al*, 2013; Paul & Hristova, 2019; Li *et al*, 2022). A heteromer taking over the function of the ancestral homomer is an example of degeneration with complementation whereby a function encoded by a single gene is now encoded by two genes. A consequence of such transitions toward heterodimers is that protein interaction networks do not benefit from the robustness usually brought about by redundancy introduced by duplication (Diss *et al*, 2017; Dandage &

Landry, 2019). Therefore, a major question these observations raise is how and why these transitions do occur.

In particular, here we are interested in understanding whether natural selection is required to drive the evolution from homodimers to heterodimers, or whether neutral evolutionary processes alone can account for this transition. Many arguments are in favor of adaptive changes. For example, different homomeric and heteromeric symmetries can facilitate specific properties such as allostery and transport (Bergendahl & Marsh, 2017). There are also compelling and potentially adaptive examples of retained heteromers. For instance, Pillai et al. (2020) thoroughly described the emergence of allosteric cooperativity in heterotetrameric haemoglobin, which is limited in homotetramers of the beta (Kurtz *et al*, 1981) or gamma subunits (Kidd *et al*, 2001). Other examples include the BfER steroid receptor that negatively regulates its paralog BfSR (Bridgham *et al*, 2008), the Mcm1 and Arg80 transcription factors whose homomers and heteromers bind specific targets (Baker *et al*, 2013), and half-ABC transporters that are only capable of transporting specific molecules out of the cell when forming heterodimers (Boncoeur *et al*, 2012). In these three examples, heteromerization between paralogs appears to currently be an important element contributing to the new function or feature. However, recent research has shown that protein interaction interfaces that do not provide an adaptive benefit can become entrenched as mutations accumulate (Finnigan *et al*, 2012; Hochberg *et al*, 2020; Schulz *et al*, 2022). A notable example is the fungal V-ATPase ring, which after a duplication shifted from a 5:1 stoichiometry to a 4:1:1 stoichiometry, resulting in increased complexity without clear changes in function (Finnigan *et al*, 2012). Thus, natural selection may not be necessary to explain why many extant heteromers were retained.

The above examples suggest that a fraction of extant heteromers of paralogs provide some adaptive benefit. At the same time, the heteromer of paralogs could have been fixed in a non-adaptive manner before the emergence of the new function. Indeed, different models have been proposed to explain how complexity could arise neutrally (Stoltzfus, 1999; Lynch, 2007; Muñoz-Gómez *et al*, 2021). In these models, the increase in complexity does not provide a fitness advantage or a disadvantage, but instead tends to become prevalent due to drift and mutational biases. Mutational biases refer to particular types of mutations (or their effects) occurring more often than others, which influence the supply of available mutations for drift and natural selection, and thus ultimately adaptation (Svensson & Berger, 2019; Cano *et al*, 2022). For instance, in the case of homomers and heteromers, there could be mutational biases that favor the assembly of one type of complex over the other. When everything else is equal, evolution tends to go in the direction of the mutational bias.

Deconvoluting the effects of mutational biases in neutral evolution and natural selection requires theoretical null models. Intuitively, if mutations naturally disrupt heteromers or favor homomerization, heteromers would tend to disappear neutrally. On the contrary, if mutations tend to favor the maintenance of the heteromers, then natural selection against these mutations or other mechanisms like compartmentalization and differential regulation would be necessary to separate the proteins in space or time and prevent the assembly of the heteromer (Marchant *et al*, 2019). The effect of individual mutations is expected to be amplified in homomers where

they are repeated by symmetry. By contrast, only a subset of the subunits in heteromers would contain a mutation. Hence, since mutational effects on binding affinity are more often destabilizing than stabilizing, one could expect homomers to be more easily disrupted. The inherent difference in expected effects of mutations could be potentiated by any mutational biases in terms of which types of mutations happen more often. Overall, the interplay between the effects of mutations, along with natural selection, should determine the fate of the paralogs. As such, we hypothesize that, in a neutral scenario, heteromers will slowly become more abundant while homomers wither away due to the accumulation of slightly destabilizing mutations.

Here, we use evolutionary simulations to examine the fate of heterodimeric complexes in a context where selection does not differentiate between homo- and heterodimers. Each step of the simulations samples biophysical effects of mutations to evaluate how they would modify the concentrations at equilibrium of homo- and heterodimers. Natural selection acts on the total amount of protein complexes formed so all three molecular complexes are free to explore a large space of possible binding equilibria neutrally within the limit set by selection. We characterize the relative impact of several parameter values that can modify the proportions of homodimers (HM) and heterodimers (HET), including changes in the synthesis rates and folding energies of individual subunits, as well as the binding affinities and specific activities of their homo- and heterodimers. Finally, we examine the relative advantages that homo- and heterodimers would need to provide to become the dominant type of complex after the duplication.

Results

The equilibrium between homomers and heteromers is highly sensitive to mutational effects on binding energy

We built a model that uses several parameters of paralogous proteins (synthesis rates, folding free energies, binding affinities, and decay rates) to estimate the concentrations of monomers and dimers at equilibrium (Figure 1A). The folding free energies (ΔG_{fold}) of the proteins are used to determine the fraction of folded protein copies (Sailer & Harms, 2017), which can later form homodimers or heterodimers based on their binding affinity (ΔG_{bind}). The concentrations of the three dimers at binding equilibrium are our trait of interest (i.e., [AA], [BB], and [AB]). We can estimate them using the different parameters because at equilibrium the rates of assembly and disassembly of dimers are identical, resulting in a system of equations. The full derivations of the systems of equations used to estimate concentrations at equilibrium before and after the duplication are shown in Supplementary Files 1 and 2, respectively. Later, in the evolutionary modeling, these parameters are allowed to evolve through mutations.

To examine how changes in these parameters will determine fitness, we defined a function that links fitness to the concentration of the total amount of protein complex formed (Figure 1B). Since we are interested in examining how neutral forces contribute to the transition from homomers to heteromers without the need for new functions, selection only acts on the total amount of complex formed (which satisfies the function) and does not distinguish between homo- and heterodimers. These assumptions will be relaxed later, as we include more parameters that could change the contribution of one type of dimer over the other to function.

We characterized the sensitivity of the post-duplication equilibrium concentrations of homo- and heterodimers to changes in the various parameter values. While preserving identical parameter values for both genes after the duplication, the relative concentrations of the three complexes will be 1AA:2AB:1BB. We then examined the post-duplication equilibrium concentration of the three complexes by testing different values for some of the parameters (Figure 1C-J). Arrows in Figures 1C-J represent examples of a mutational trajectory to illustrate how changes in the ΔG_{fold} or ΔG_{bind} parameters affect the concentrations of complexes at equilibrium, the total activity, and the fitness. We first studied the effects of different combinations of folding free energy values (Figure 1C-F) around the typical value of -5 kcal/mol (Pace, 1975; Plaxco *et al*, 2000). As expected, destabilizing the fold of only one of the paralogs led to a decrease in the number of available copies of that protein. As a result, the concentrations of its corresponding homodimer and the heterodimer decreased as well, with an increase in the concentration of the other homodimer (Figure 1C-D). We note that the percentage of heterodimers never exceeded 50% when only folding energies changed, and that it was quickly reduced when either subunit was significantly destabilized. Indeed, destabilizing either or both of the protein subunits ($\Delta G_{fold} > 0$) led to a reduction in the total concentration of dimers, and thus in their total activity (Figure 1E) and fitness (Figure 1F). Overall, the effect of folding free energy on the balance between homo- and heterodimers was moderate as long as $\Delta G_{fold} < 0$ for both subunits.

6

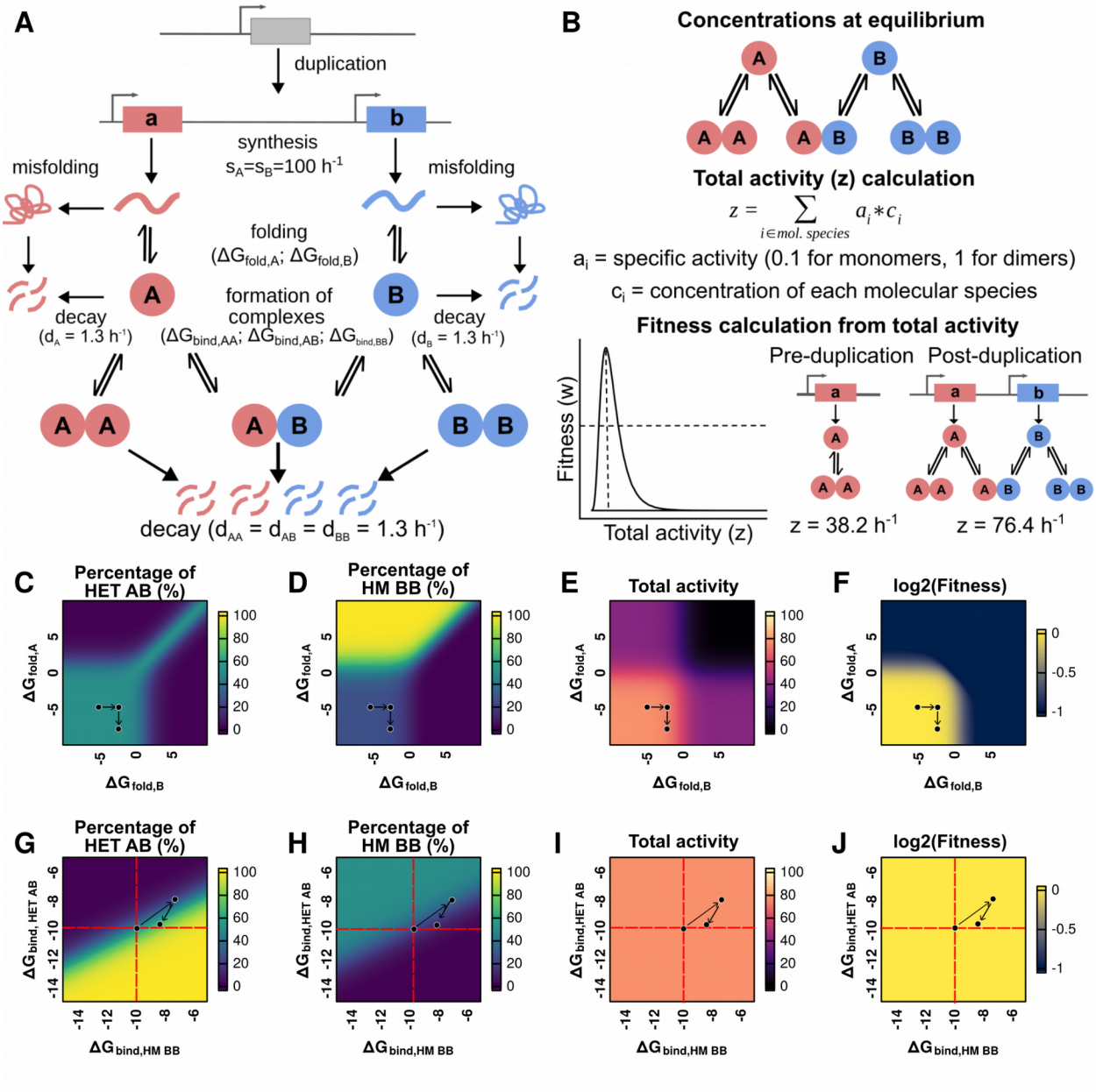

Figure 1. Changes to folding free energy and binding affinity modify the concentration of each dimer and the fitness of the system.

A. Post duplication system. Paralogous proteins are produced with synthesis rates s_A and s_B. Synthesis encompasses both transcription and translation, which are not considered separately. The probability of correct folding is calculated based on the folding free energy (ΔG_{fold}) (see Methods). Misfolded proteins are removed from the system. Folded proteins can assemble into homo- or heterodimers based on binding free energies ($\Delta G_{bind,HM\ AA}$, $\Delta G_{bind,HET\ AB}$, $\Delta G_{bind,HM\ BB}$).

B. The concentrations of each molecular species (monomers, homodimers, and heterodimers) are estimated at equilibrium. Total protein activity is calculated by multiplying the equilibrium concentrations by their specific activity (0.1 for monomers, 1 for both homodimers and the heterodimer). Fitness is estimated based on the total protein activity using a lognormal function given by parameters alpha and beta. With the parameters for synthesis rates and decay rates shown in figure 1A, the estimated values of

7

total activity for the system before and after the duplication corresponded to 38.2 h^{-1} and 76.4 h^{-1}.
C-F. Effect of variation in the ΔG_{fold} for each monomer on the percentage of heterodimer (HET AB) (C), percentage of one of the homodimers (HM BB) (D), the total activity (E), and fitness (F) of the system. Fitness is estimated using a lognormal distribution with the optimum (alpha value) set to a total activity of 80 (see Figure 1B). Arrows represent an example of a mutational trajectory.
G-J. Effect of variation in $\Delta G_{bind,HET\ AB}$ and $\Delta G_{bind,HM\ BB}$ on the percentage of the heterodimer (HET AB) (G), percentage of one of the homodimers (HM BB) (H), and the total activity (I), and fitness (J) of the system. For panels G-J, $\Delta G_{bind,HM\ AA}$ was kept constant at -10 kcal /mol. Arrows represent an example of a mutational trajectory.

We then studied the effects of changes to binding affinity in their typical range of values, centered around -10 kcal/mol (Choi *et al*, 2015; Jankauskaitė *et al*, 2018). Figures 1G-J show how changes in the binding affinities of the heterodimer ($\Delta G_{bind,HET\ AB}$) and one of the homodimers ($\Delta G_{bind,HM\ BB}$) impact the overall system. Throughout this analysis, the binding affinity of the second homodimer ($\Delta G_{bind,HM\ AA}$) is kept constant at -10 kcal/mol to allow representing the data in two dimensions. As expected, the heterodimer was enriched if it became the complex with the strongest binding affinity and depleted if it had the weakest binding affinity (Figure 1G-H, Figure S1A-D). Interestingly, there are regions in the solution space in which most of the available subunits assembled into homodimers although one of the homodimers had a slightly weaker binding affinity than the heterodimer (Figure S1E). In this case, the available copies of one of the proteins would be depleted by fast assembly of their homodimer, so the copies of the second protein would assemble into their respective homodimers. On the contrary, heterodimers were enriched when their binding affinity was slightly weaker than that of one of the homodimers but much stronger than that of the second homodimer (Figure S1F). Here, any exchange of subunits between the heterodimer and the stronger homodimer would release subunits of the weaker homodimer, leading to an imbalance of concentrations of free subunits. Thus, equilibrium would favor strong heterodimers over a mixture of strong and weak homodimers. Importantly, in the range of values tested and assuming the specific activities of homo- and heterodimers are identical, the total activity and fitness of the system remain unchanged despite shifts in the concentration of each dimer (Figures 1I-J). The effects of an extended range of values of binding energy are shown in Figure S2. When one of the homodimers is completely destabilized, the system is dominated by the equilibrium between the second homodimer and the heterodimer (Figure S2A-B). In this case, if the heterodimer is also destabilized, the remaining homodimer can approach 100% of the dimers. Such destabilization would lead to a return of the pre-duplication state of only one homodimer, with a corresponding loss in total activity (Figure S2C) and fitness (Figure S2D) of the system. Overall, the post-duplication equilibrium is highly sensitive to changes in binding affinity when all other parameters remain constant: there is a narrow region where the concentrations of homo- and heterodimers stay close to the original 1AA:2AB:1BB ratios, but small changes can lead to drastic changes in the concentration of each dimer.

The solution space of the system of equations shows that directly after duplication, the equilibrium concentrations of each dimer are particularly sensitive to mutational effects on binding affinity. Differences between the binding affinity of homo- and heterodimers in the range of 0.5 - 1.0 kcal/mol are sufficient to drastically alter the representation of the heteromer in the

234 system (Figure 1G). This is supported by empirical observations. Studies show that homomeric
235 specificity can be achieved with just 1-3 substitutions (Ashenberg *et al*, 2011; Garcia-Seisdedos
236 *et al*, 2017; Stutz & Blein, 2020; Emlaw *et al*, 2021) and marginal differences in binding affinity
237 (Hochberg *et al*, 2018). On the other hand, there are regions of the solution space that are much
238 less sensitive to these mutational effects, for example, when the difference in ΔG_{bind} between
239 the homodimers and the heterodimer is already very large. These results are in agreement with
240 previous models on the energetic cost of homomerization derived using a different approach
241 (Hochberg *et al*, 2018). An important consideration is that these changes in binding affinity alter
242 the representation of each dimer in the system, but do not modify the total concentration of
243 complexes, as seen in Figure 1I. Thus, there would be many ways for the cell to provide the
244 same total concentration of complexes, all of which could have the same fitness if every dimer
245 has the same specific activity (Figure 1J). While the landscapes presented on Figure 1 help
246 visualize the effect of changes to one parameter at a time, the fate of modern paralogs
247 (Marchant *et al*, 2019; Mallik & Tawfik, 2020) is a product of the co-evolution and correlation of
248 many parameters (synthesis, folding, binding, activity, etc.). Simulating evolution of these
249 landscapes therefore needs to be based on the actual distributions of effects, which can vary
250 from one protein to another. Importantly, these observations show that the system could
251 theoretically deviate strongly from the starting relative concentrations while keeping the same
252 overall performance and this, in a directional manner, if mutations have biased effects in one
253 direction or the other.

254 **Evolutionary simulations show a general bias toward heterodimers replacing the**
255 **ancestral homodimer**

256 We used the above model to simulate the evolution of the post-duplication equilibrium between
257 homo- and heterodimers as mutations accumulate (Figure 2A). Mutations lead to changes in the
258 protein sequence, which can affect the binding affinity and the folding free energy of proteins. To
259 derive the distributions of mutational effects, we sampled a set of 104 homodimers with crystal
260 structures from the Protein Data Bank (Berman *et al*, 2000) and simulated the effects of all
261 possible single amino acid substitutions on folding free energy and binding affinity with FoldX
262 (Delgado *et al*, 2019) (see Methods). Briefly, entries from the PDB were chosen if their
263 structures were solved by X-ray crystallography, annotated as homomers, having exactly the
264 same or no missing residues, and with sequence lengths between 60 and 450 residues. From
265 the resulting set of structures, we selected entries from the major ECOD architecture types
266 (Cheng *et al*, 2014) so that we would have chosen at least seven for each of them. Similarly, we
267 clustered these proteins at 40% sequence identity with CD-Hit (Li & Godzik, 2006; Fu *et al*,
268 2012), and selected one representative protein from each cluster.

269 We used our model and the dataset of structures to simulate the post-duplication evolution of
270 pairs of paralogs. We considered two different regimes for our simulations: parametric, in which
271 we sampled mutational effects from multivariate normal distributions with different parameters
272 based on the pooled structural data; and single structure, in which mutational effects are
273 sampled directly from the distribution of effects of the corresponding structure. Since mutations
274 can affect binding affinity and folding free energy at the same time, we derive multivariate

normal distributions for the effects of mutations based on the pooled data. These distributions have the following parameters, all in kcal/mol: for $\Delta\Delta G_{bind, HET}$, mean = 0.2, standard deviation = 1.2 (denoted as N(0.2, 1.2)); for $\Delta\Delta G_{bind, HM}$, N(0.4, 2.4); and for $\Delta\Delta G_{fold}$, N(2.6, 4.6). Additionally, we imposed correlations between these distributions following our observations with the pooled data: r = 0.9 between $\Delta\Delta G_{bind, HET}$ and $\Delta\Delta G_{bind, HM}$ (Figure S3A), r = 0.3 between $\Delta\Delta G_{bind, HET}$ and $\Delta\Delta G_{fold}$ (Figure S3B), and r = 0.3 between $\Delta\Delta G_{bind, HM}$ and $\Delta\Delta G_{fold}$ (Figure S3C). We annotated figure panels for results for parametric simulations with a computer cartoon and results for single structure simulations with a protein dimer cartoon throughout the rest of the text.

Each step of the simulation represents a mutational event. Importantly, the underlying distribution from which the effects of mutations are sampled is kept constant. As discussed later, we apply this simplifying assumption to keep the simulations scalable because, while the effects of new individual mutations are contingent on previous ones, it is unclear whether the shape of the global distribution changes. Once a mutational effect is sampled, we update all relevant binding affinities and folding energies and recalculate the concentrations at equilibrium for monomers and dimers. Next, we use the equilibrium concentrations to obtain the total activity of the system. Fitness is then estimated using a lognormal function given by two parameters: alpha (the value of total activity that maximizes fitness) and beta (the fitness corresponding to activity values of half and twice the value of alpha, beta was set to 0.5 for all simulations). We tested our simulations with two different values for alpha to consider two different scenarios: one in which the total activity after the duplication (76.4 h^{-1}) is very close to the optimal value (alpha = 80 h^{-1}), and one in which it overshoots the optimal value (alpha = 60 h^{-1}). Finally, fitness is used to calculate the probability of fixation for that mutational effect. Once a mutational effect fixes or is rejected, the simulation continues with the next sampling step. Each simulation was run with 50 replicates and allowed to continue until 200 mutations were fixed. Although some of the proteins tested are shorter than 200 residues, the sequences of paralogs maintained about 50% identity with the WT sequence and more than 30% sequence identity with one another by the end of the simulations. These measures are consistent with real-world scenarios where more than half of *S. cerevisiae* and *E. coli* paralogous pairs exhibit ≥30% identity (Mallik & Tawfik, 2020). Since the results for the two scenarios (alpha = 60 h^{-1}, alpha = 80 h^{-1}) generally agreed, the results with alpha = 80 h^{-1} are shown in the main text and those with alpha = 60 h^{-1} are shown in the supplementary materials.

We tested how changes in the parameters of the distribution of mutational effects of the homodimer affected the simulation outcome (Figure 2B, Figure S4). We allowed the parameters for the distribution of effects on $\Delta\Delta G_{bind, HM}$ to change while the distribution for $\Delta\Delta G_{bind, HET}$ was given by N(0.2, 1.2) and the distribution for $\Delta\Delta G_{fold}$ was given by N(2.6, 4.6). As expected, homodimers dominate when the average mutation is more destabilizing for the heterodimer than for the homodimer. Homodimers also dominate when the variance in mutational effects on $\Delta\Delta G_{bind, HM}$ is high, since this allows for extreme stabilizing effects on the homodimer. High variance also allows extreme destabilizing effects to be sampled often but they would be likely eliminated by selection because they also affect the total concentration of the complexes. Interestingly, simulations with parameters along the diagonal of Figure 2B tend to maintain both

homo- and heterodimers, with two conditions of particular interest indicated with a circle and a triangle. The circle indicates the simulation in which mutational effects are the same for homo- and heterodimers, while the triangle represents the simulation in which mutational effects on the homodimer are double of those on the heterodimer as in our data derived with FoldX. The preservation of the mixture of homo- and heterodimers in these two conditions suggests that the mere doubling of mutational effects on the homodimer does not lead to an increase in the concentration of heterodimers, as long as effects are sampled from correlated ideal normal distributions. Thus, our parametric simulations show that when none of the dimers offers an advantage over the others, biases in the distribution of available mutational effects alone can determine which dimer dominates at the end of the simulation.

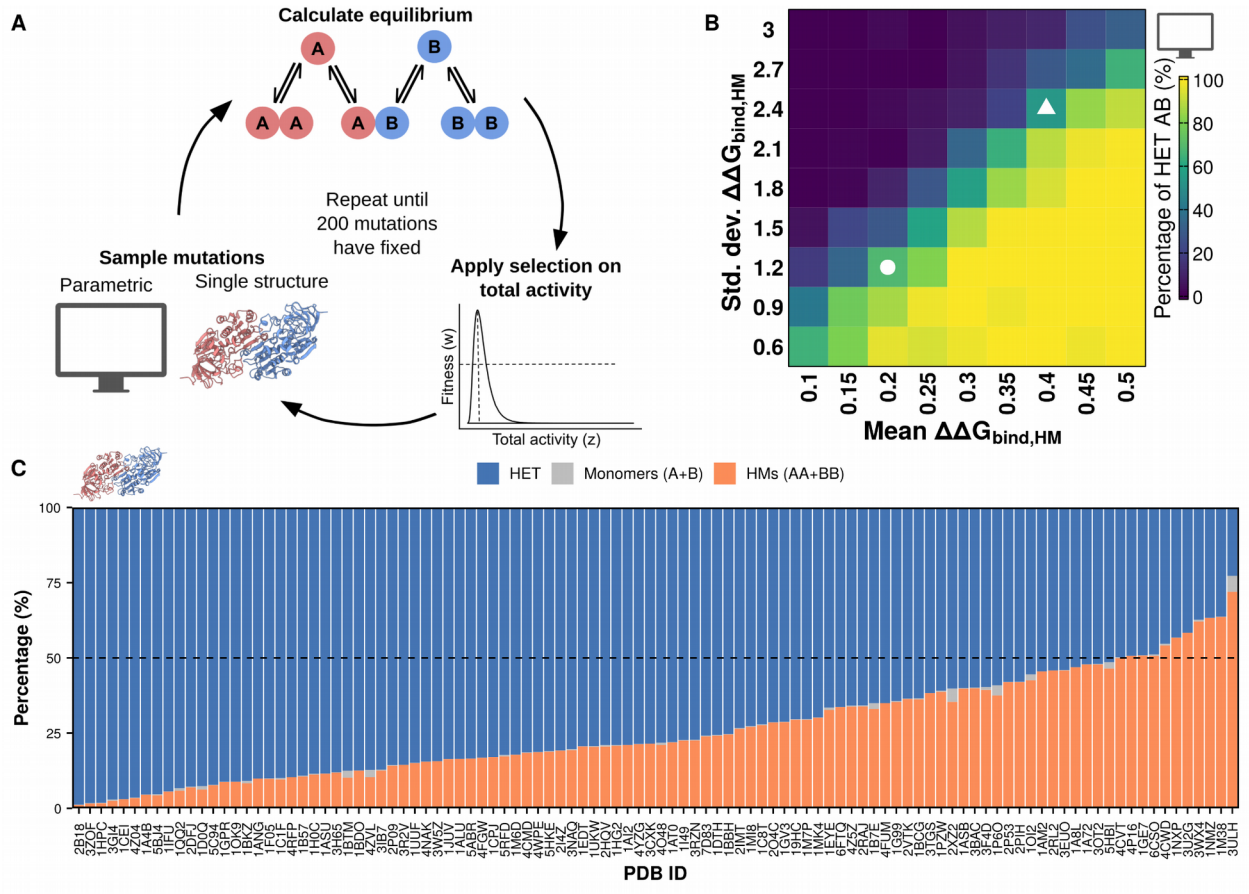

Figure 2. Biases in the distribution of effects on mutations on binding affinity can drive enrichments of homomers or heteromers.
A. Overview of the simulation workflow. Homodimers from the PDB were used to infer distributions of mutational effects for two regimes of simulations: those with distributions based on the pooled data (parametric) and those using data for a single structure. Mutations are sampled from these distributions, after which the concentrations of dimers and monomers at equilibrium are recalculated. Selection is applied based on the total activity in the system. Simulations continued until 200 mutations were fixed. The structure for 1A72, used as the cartoon for the single structure simulations, was visualized with ChimeraX (Pettersen *et al*, 2021).
B. Percentage of heteromers at the end of the simulations with each set of parameters for the

homodimers (average of 50 replicates, 200 mutations fixed for each). The white circle indicates the condition in which $\Delta\Delta G_{bind,HET}$ and $\Delta\Delta G_{bind,HM}$ are equally distributed (N(0.2, 1.2)). The white triangle indicates the condition in which the distribution for $\Delta\Delta G_{bind,HM}$ uses the same parameters calculated when considering all the sampled structures (N(0.4, 2.4)).
C. Average percentages of heterodimers, homodimers, and monomers for each of the PDB structures at the end of the simulations. The dashed line indicates the starting point at 50% heterodimers and 50% homodimers (25% of each homodimer).

We next set out to test our simulation system with the direct distributions of mutational effects for each of the PDB structures sampled. Simulations were run with the estimated distributions of mutational effects for 104 structures of homodimeric proteins available in the PDB. Replicates of the same simulation followed slightly different trajectories due to the inherent stochasticity of the process. Nevertheless, we observed that different protein structures were associated with different average outcomes, implying that structural features can encode a homodimer- or heterodimer-dominant fate after duplication (Figure 2C, Figure S5). Strikingly, for most of the protein structures tested, the average concentration of heterodimers at the end of the simulations was higher than the starting 50%. Indeed, for 66 structures (63.4%) the final concentration of heterodimers was higher than 70%, as opposed to only 1 structure (1%) for which the final concentration of homodimers was higher than 70%. For the remaining 37 structures (35.5%), the final concentrations stayed closer to the initial equilibrium, with neither heterodimers nor homodimers enriched beyond 70%. The enrichment of heteromers tended to occur relatively early in the simulations, with some structures showing high heterodimer concentrations after fewer than 100 mutations had been fixed (Figure S5). This is consistent with our previous finding that heteromerization also dominates in recently duplicated yeast paralogous pairs that have retained high sequence identity (Marchant *et al*, 2019; Mallik & Tawfik, 2020). These observations suggest there exists a neutral bias toward the replacement of ancestral homodimers by heterodimers, although independent identical events might reach different outcomes.

In our previous simulations, the optimum value for total activity (alpha = 80 h^{-1}) was slightly higher than the total activity directly after the duplication. The results of simulations where the duplication overshoots the optimum (alpha = 60 h^{-1}) correlated well (r = 0.85), although simulations with alpha = 60 h^{-1} consistently yielded slightly lower percentages of heterodimers (Figure S6A-B). Considering that the post-duplication total activity is 76.4 h^{-1}, simulations with alpha = 60 h-1 required a reduction of total activity to approach the optimum fitness. Indeed, at least one of the subunits was quickly destabilized in these simulations (Figure S6C), which did not happen in the simulations with alpha = 80 h^{-1} (Figure S6D). The quick destabilization observed in the simulations with alpha = 60 h^{-1} occurred at the same time as an initial decrease in the concentration of heterodimers since the available concentrations of free subunits would be different (Figure S6E). As the simulations advanced, the concentrations of heterodimers increased, both when alpha = 60 h^{-1} and when alpha = 80 h^{-1} (Figure S6E-F). Thus, our simulations show the inherent bias toward the increase in the concentration of heterodimers is robust to the position of the fitness optimum.

12

These results motivated us to identify structural properties that may influence the outcome of the simulations. First, we focused on the interfaces of our set of PDB structures. We looked at the relative size of the interface core (Figure S7A), the overall stickiness of the interface (Figure S7B), the proportion of interface core residues that are involved in homotypic contacts (Figure S7C), and the overall secondary structure of the interface (Figure S7D). However, none of these interface parameters showed a clear association with the outcome of the simulations. We extended our secondary structure analysis to the ECOD architectures (Cheng *et al*, 2014) of our protein set (Figure S7E, Table S1). Outcomes of simulations with structures with similar ECOD architectures were highly variable, suggesting that the general structural parameters we tested are not sufficient to make an association with the bias toward heterodimers. Similarly, we observed that modifying the starting parameters of subunit folding free energy and binding affinity tended to have little effect on the most frequent outcome of simulations with a given structure (Figure S8). These results suggest that the outcome of the simulations depends on properties of the distribution of mutational effects that are not directly derived from these structural features.

Weak but constant mutational biases influence the outcome of evolution

We reasoned that, although the distributions for all proteins in our set are very similar, they might differ with respect to the availability of outliers or pervasive biases with small magnitude in terms of folding or binding energies, which would then drive evolution in one particular direction. Considering that changes in ΔG_{fold} never lead to an increase in the concentration of heterodimers (Figure 1C), we focused our analysis on the effects on ΔG_{bind}. For simplicity, we first compared the distributions of available and fixed mutational effects on $\Delta G_{bind,HET}$ and $\Delta G_{bind,HM}$ for the structures with the two most extreme outcomes (2B18 as heterodimer-dominant and 3ULH as homodimer-dominant) (Figure 3A-B). As noted above, mutational effects on $\Delta G_{bind,HET}$ and $\Delta G_{bind,HM}$ are highly correlated for both structures, and fixed mutations were not restricted to any single part of the distribution. Thus, we hypothesized that proteins that are enriched for heterodimers in the simulations might have access to more mutations with slight deviations from the expected diagonal that favor the heterodimer, which would gradually accumulate as the simulation progresses. For example, a mutation that is below the diagonal in figure 3A-B would destabilize the heterodimer less (or stabilize it more) than expected based on the effect on the homodimer, whereas mutations above the diagonal would favor the homodimer. We calculated these deviations from the diagonal as follows:

$$residual = \Delta\Delta G_{bind,HET\,AB} - 0.5 * \Delta\Delta G_{bind,HM\,AA}$$

13

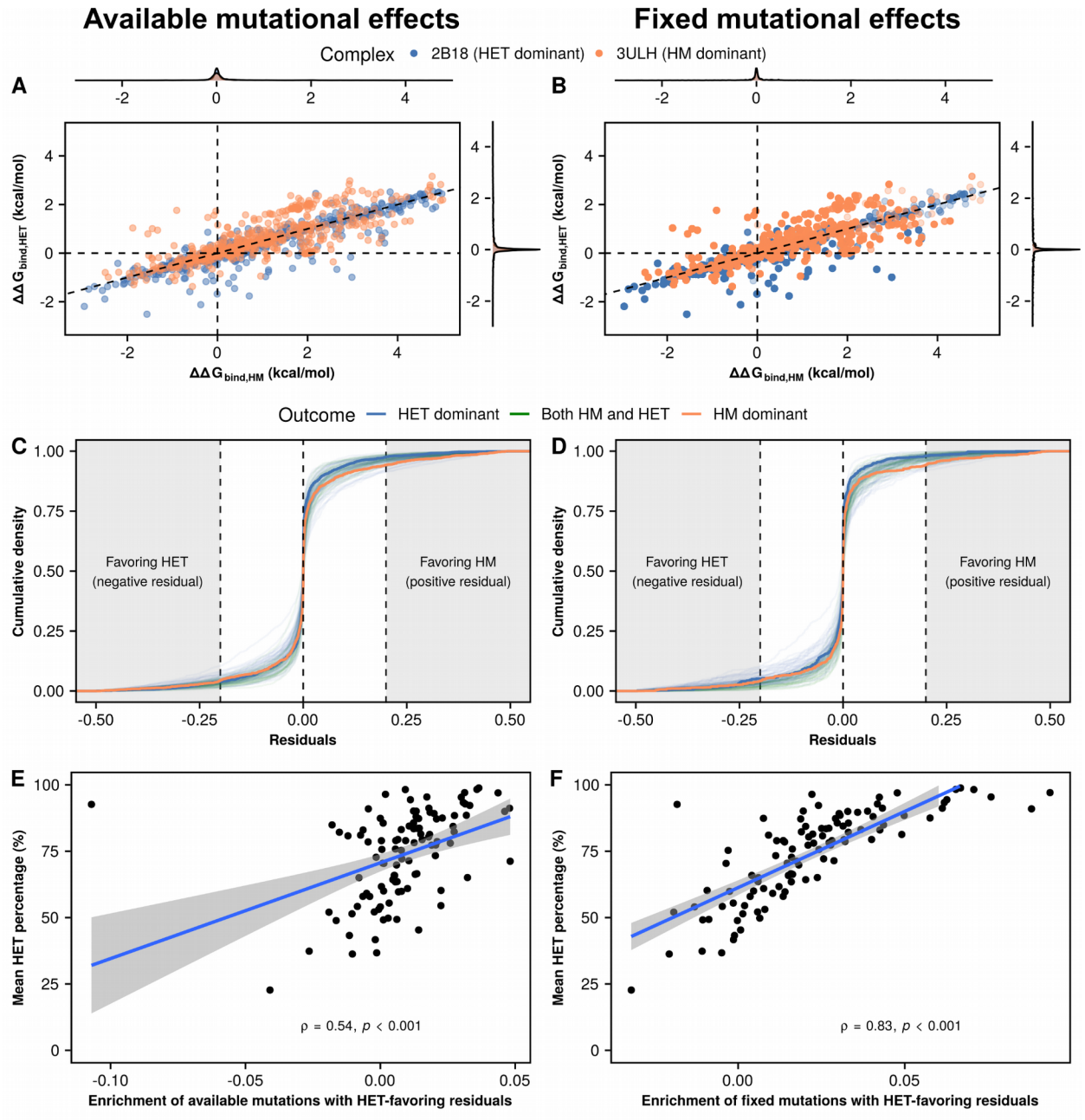

Figure 3. Slight deviations from the diagonal (residuals) are associated with the outcome of the simulations.

A-B. Distributions of available (A) and fixed (B) mutational effects on $\Delta G_{bind,HET}$ and $\Delta G_{bind,HM}$ for the two proteins with the most extreme outcomes in figure 2C: 2B18 (heterodimer-dominant) and 3ULH (homodimer-dominant). The diagonal ($\Delta\Delta G_{bind,HET} = 0.5 * \Delta\Delta G_{bind,HM}$) is shown to illustrate the expectation of mutations on the heterodimer having half of the effect of mutations on the homodimer.

C-D. Distributions of available (C) and fixed (D) residuals with respect to the expectation for each of the 104 structures. Colors indicate mean outcomes for each structure: HET dominant (heterodimer > 70% of dimers), HM dominant (homodimer > 70% of dimers), both HM and HET (rest of cases). The thicker blue and orange lines represent 2B18 and 3ULH, respectively. Shaded regions on the left and right indicate mutations whose residuals have a magnitude of at least 0.2 kcal/mol favoring either the heterodimer

14

(negative values) or the homodimer (positive values).
E-F. Correlation between enrichment of available (E) and fixed (F) mutations with residuals favoring the heterodimer and the mean percentage of heterodimers at the end of the simulations. The enrichment of heterodimer-favoring residuals is calculated as the density of mutations with residuals smaller than -0.2 kcal/mol minus the density of mutations with residuals greater than 0.2 kcal/mol.

The cumulative distributions of residuals of available and fixed mutations show minor differences overall (Figure 3C-D). While comparing 2B18 (the most heterodimer-dominant structure) to 3ULH (the most homodimer-dominant structure) reveals that 3ULH has a slightly higher density of mutations with positive (homodimer-favoring) residuals, the effect is not as clear for the rest of the structures. To have a finer resolution, we defined an enrichment of heterodimer-favoring residuals as the percentage of residuals with magnitudes below -0.2 kcal/mol (heterodimer-favoring) minus the percentage of residuals with magnitudes above 0.2 kcal/mol (homodimer-favoring). Structures with a higher enrichment of heterodimer-favoring mutations are the ones with the highest concentrations of heterodimers at the end of the simulations (Figure 3E-F). We note that the available enrichment of heterodimer-favoring mutations is amplified in the mutations that fix throughout the simulations.The results of repeating this analysis with other thresholds for the residuals are shown in Table S2 ($0.39 < r < 0.54$ for available mutations, $0.67 < r < 0.83$ for fixed mutations). Indeed, the cumulative sum of residuals fixed up to a particular point in the simulations explains very well the observed percentage of heteromers (Figure S9). We repeated the previous analyses with only the structures evaluated as very high quality in the QSBio database (37 out of 104 structures) (Dey *et al*, 2018). Simulations with these structures also led to an enrichment of heterodimers due to mutational biases (Figure S10), although the increase in heterodimer concentration was less drastic than in the full dataset. As a result, small but consistent mutational biases appear to be responsible for the increase in the concentration of the heterodimer, even without selection explicitly favoring it.

Differences in synthesis rate and specific activity can reverse the bias toward heterodimers

Our results so far show that the concentration of heterodimers relative to the homodimers after duplication is expected to increase even in the absence of selection favoring this complex over the homodimers. However, a large fraction of duplicated homodimeric proteins do not maintain their heterodimers. Other forces could thus counterbalance this inherent mutational trend. These include differences in compartmentalization, expression profiles, and specific activities. Paralogs that are separated into different compartments, such as yeast thioredoxin reductases TRR1 (cytosolic) and TRR2 (mitochondrial), do not interact *in vivo* despite still being capable of doing so *in vitro* (Oughtred *et al*, 2021; Mallik *et al*, 2022). For differentially expressed paralogs, such as *E. coli* LYSS (constitutive) and LYSU (heat-induced) (Brevet *et al*, 1995), equilibrium shifts toward the homodimer of the more highly abundant protein. Differences in the specific activity of homomers and heteromers would help selection distinguish between the two of them to maintain a particular total activity in the system.

We therefore examined the impact of differential synthesis rates and specific activities on the

outcome of evolution. We do not model the case where one of the dimers could evolve a novel function, because it would require multiple additional considerations. For example, the system would need to describe and deconvolute mutational effects on each of the two functions. Also, the two functions could have different weights in the fitness calculations. Additionally, those considerations should be specific to each protein, unlike folding and binding which are common physical properties of all the dimers we consider.

We first used our equations to characterize the effect of changes in relative synthesis rates between paralogs. We observed that the concentration of the heterodimer is maximized when synthesis rates were identical (Figure 4A). Conversely, the concentration of either homodimer was maximized as the synthesis rate of its subunits increased beyond that of its paralog (Figure 4B). The total activity of the system increased with the synthesis rate of one of the paralogs (Figure 4C), which initially led to higher fitness as total activity approached the optimum of our fitness function (alpha = 80 h^{-1}). However, fitness decreased as total activity went beyond the optimum (Figure 4D). Since many paralogous proteins are differentially expressed (Gout *et al*, 2010; Gout & Lynch, 2015; Aubé *et al*, 2023), expression divergence could counteract mutational biases that favor heterodimers. However, the extent of this effect would depend on the relative frequencies of mutational effects on synthesis rates versus the coding sequence, as well as the fitness effects of changes in the total activity of the system due to the total amount of protein copies produced.

16

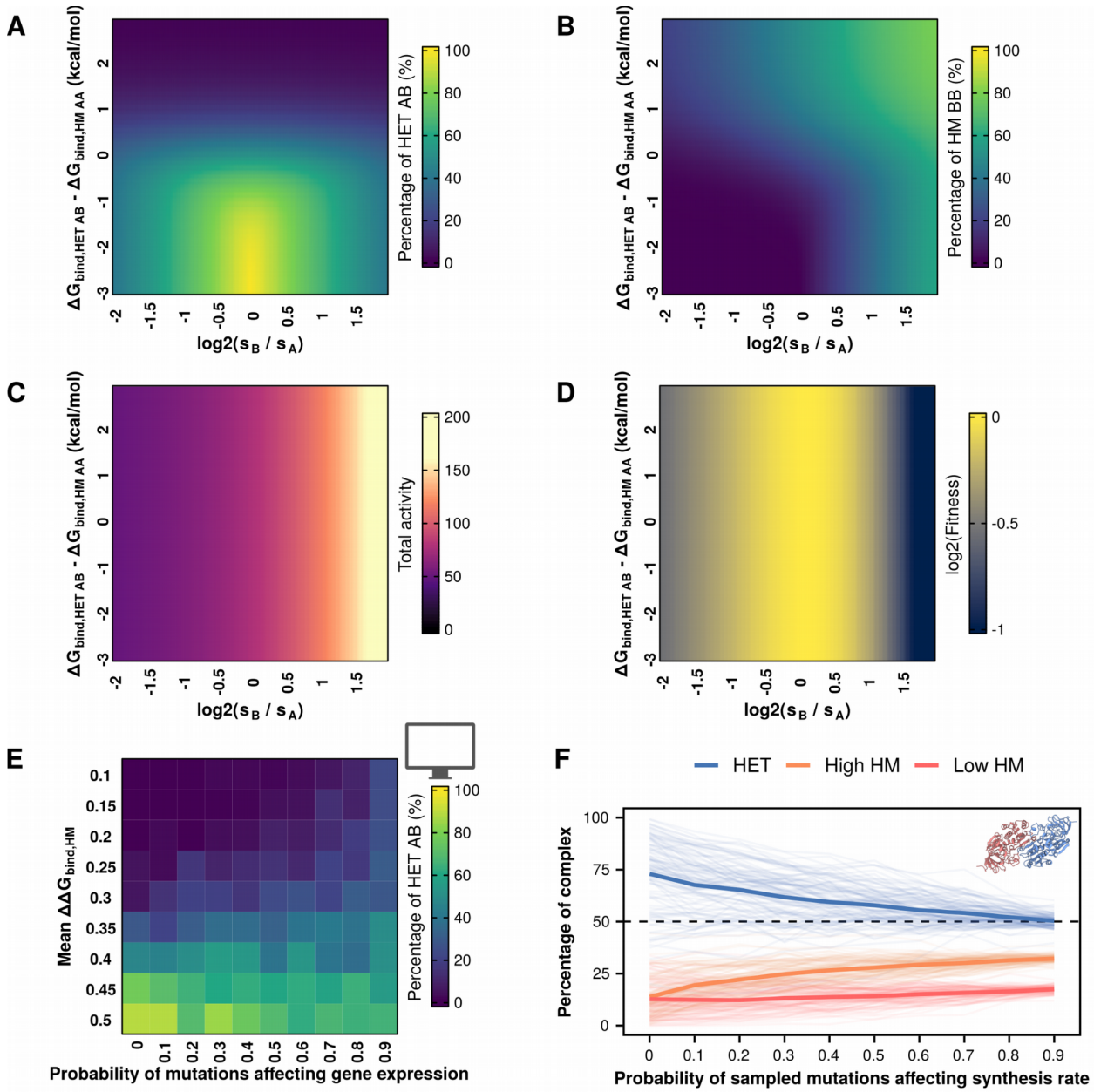

481 **Figure 4. Allowing changes in synthesis rates can limit the bias toward heterodimers.**
482 **A-D.** Percentage of heterodimers (A), one of the homodimers (B), total activity (C), and fitness (D) as a
483 function of the ratio of synthesis rates and differences between $\Delta\Delta G_{bind,AB}$ and $\Delta\Delta G_{bind,AA}$. In panels A-D,
484 s_A, $\Delta\Delta G_{bind,AA}$, and $\Delta\Delta G_{bind,BB}$ remain constant throughout. Changes in the y-axis indicate changes in
485 $\Delta\Delta G_{bind,AB}$, with all three values ($\Delta\Delta G_{bind,AA}$, $\Delta\Delta G_{bind,AB}$, $\Delta\Delta G_{bind,BB}$) being identical at zero.
486 **E.** Percentages of heterodimers at the end of parametric simulations allowing changes in synthesis rates
487 and varying mean effects of mutations on homodimers.
488 **F.** Percentages of heterodimers and each of the two homodimers for each of the 104 tested structures
489 when simulations include different probabilities of mutations affecting synthesis rates. The two
490 homodimers were distinguished based on their abundance, such that high HM refers to the one with the
491 higher concentration and low HM to the one with a lower concentration.

492 Mutations can affect synthesis rates in multiple ways. For example, they could affect binding of
493 transcription factors to a promoter or translation rates (Hausser *et al*, 2019; Verma *et al*, 2019;
494 Kemble *et al*, 2020; Roos & de Boer, 2021; Aubé *et al*, 2023). Here, we did not distinguish
495 between each of these individual mechanisms but considered synthesis as encompassing all
496 possible effects. We considered the distribution of the effects of mutations on gene expression
497 observed by Metzger et al. (2016) for the TDH3 promoter. We added a new parameter
498 representing the probability of mutations affecting synthesis rates (p_{exp}) in the simulations. In
499 these cases, we sampled the effect of mutations on synthesis rates from a separate skew-
500 normal distribution (mean = 0, variance = 0.025, skew = -0.125) following the Metzger et al.
501 (2016) data. These effects were considered to be multiplicative, i.e. the current synthesis rate at
502 the corresponding step in the simulations would be multiplied by the value sampled from the
503 distribution of mutational effects on synthesis rates.

504 Since promoter sequences can have widely variable rates of evolution (Young *et al*, 2015,
505 2022), we proceeded to repeat our simulations with different probabilities of mutational effects
506 affecting synthesis rates. In these parametric simulations, we observed that higher probabilities
507 of mutations affecting synthesis rates generally led to less extreme outcomes in terms of
508 homodimer or heterodimer dominance (Figure 4E, Figure S11), even when mutational effects on
509 binding affinity were skewed against either of them. At higher probabilities of mutations affecting
510 synthesis rate, the concentration of the heterodimer remained in the range between 40 - 60% of
511 the complexes. Similarly, the bias toward heterodimers observed for the simulations with the
512 simulations for individual PDB structures became considerably weaker as the probability of
513 mutations affecting synthesis rates increased (Figure 4F). We note that the synthesis rates of
514 the two paralogs did not diverge considerably in the simulations (in the most extreme case, with
515 mutations having p_{exp} = 0.9, median divergence in synthesis rates for the same replicate = 26.1
516 h^{-1}, interquartile range = [12.07 h^{-1}, 44.6 h^{-1}]) (Figure S12). Such differences in protein
517 abundance represent a log2 fold change of 0.35, which is within the range observed for
518 paralogous proteins (Aubé *et al*, 2023). We repeated these simulations setting the optimal
519 activity value (alpha) to 60 h^{-1} so that the duplication would overshoot the optimum and obtained
520 similar results, albeit with slightly lower concentrations of heterodimers (Figure S13).

521 Overall, allowing changes in synthesis rates tended to preserve both homo- and heterodimers.
522 This effect can be understood as two components. First, divergence in synthesis rates would
523 naturally shift equilibrium away from the heterodimer and toward the homodimer of the more
524 abundant protein (Figure 4A-B). Since fitness was sensitive to synthesis rates (Figure 4D), it
525 was likely that an increase in the synthesis rate of one protein would be followed by a decrease
526 in the synthesis rate of its paralog, even if these differences in synthesis rates were moderate
527 (Figure S12). Second, because mutations in our simulations either affect synthesis rates or the
528 protein sequence, accelerating the evolution of synthesis rates implied decelerating the
529 evolution of the coding sequence and limiting the accumulation of mutational biases that led to
530 the enrichment of the heterodimer. Our result that allowing changes in synthesis rates limits the
531 bias toward heterodimers can help explain why extant paralog pairs often keep both homomers
532 and heteromers (Marchant *et al*, 2019; Mallik & Tawfik, 2020), considering that the abundances
533 of paralogs often diverge (Gout *et al*, 2010; Gout & Lynch, 2015; Aubé *et al*, 2023).

We then characterized the effect of changes in the specific activity of the homodimers or the heterodimers. In real biological systems, the expectation would be that these specific activities start out as being identical and then slowly diverge as mutations accumulate. However, since the relationship between sequence and function is complex and specific to each protein, we decided to use the simplifying assumption that specific activities would differ directly from the beginning. In these simulations, the more active dimer always has a specific activity of 1, whereas the less active dimer has a specific activity between 0.2 and 0.9. We define a HET activity bias as the difference in specific activities. For example, a -10% HET activity bias indicates the heterodimer is less active than the homodimers (specific activities of 0.9 for heterodimers and 1 for homodimers), whereas a 10% HET activity bias indicates the heterodimer is more active (specific activities of 1 for heterodimers and 0.9 for homodimers). As expected, changes in the specific activity did not affect the assembly of complexes (Figure 5A-B), since it is determined by binding affinities and the concentrations of properly folded subunits. However, they did have an impact on the total activity of the system (Figure 5C) and fitness (Figure 5D). Total activity was maximized when the most active dimer was the most abundant one (top left and bottom right corners of Figure 5C). Since the specific activity of homodimers or heterodimers never exceeded 1 with our definition of HET activity bias, fitness was maximized in the same regions where activity was maximized (Figure 5D), although the landscape would be different if we allowed values higher than 1. Thus, the solution space of the system of equations shows that allowing differences in specific activity can promote selection for either homodimers or heterodimers.

19

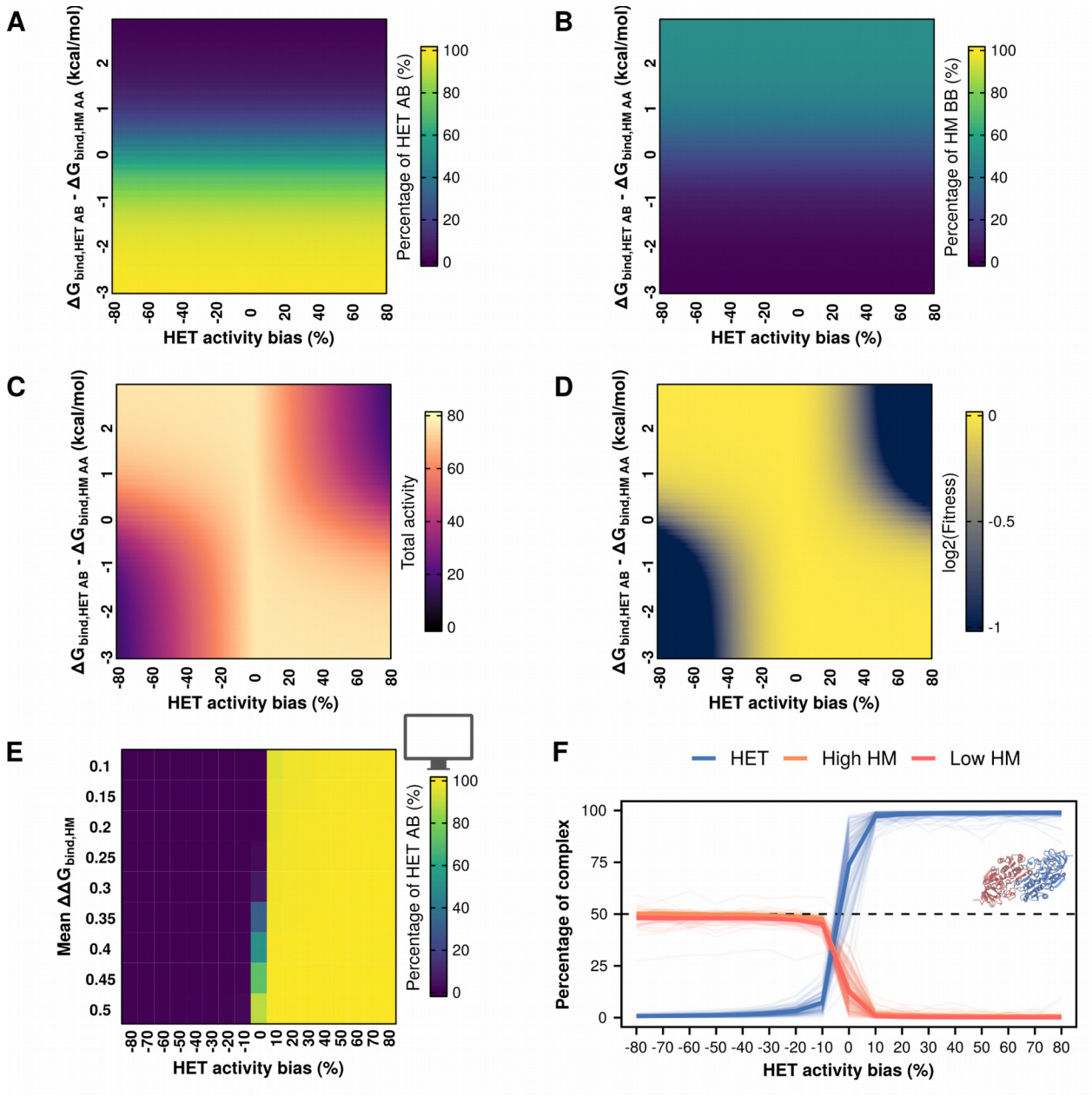

Figure 5. Differences in specific activities of homodimers and heterodimers can revert the observed bias towards heterodimers.

A-D. Percentage of heterodimers (A), one of the homodimers (B), total activity (C), and fitness (D) as a function of differences in specific activity and differences between between $\Delta\Delta G_{bind,HET\ AB}$ and $\Delta\Delta G_{bind,HM\ AA}$. In panels A-D, $\Delta\Delta G_{bind,HM\ AA}$ and $\Delta\Delta G_{bind,HM\ BB}$ remain constant throughout. Changes in the y-axis indicate changes in $\Delta\Delta G_{bind,AB}$, with all three values ($\Delta\Delta G_{bind,HM\ AA}$, $\Delta\Delta G_{bind,HET\ AB}$, $\Delta\Delta G_{bind,HM\ BB}$) being identical at zero.

E. Parametric simulations using differences in the specific activities of homo- and heterodimers and varying mean effects of mutations on homomers. HET activity bias indicates a percentage decrease (negative values) or increase (positive values) of the heterodimer activity with respect to the homodimer activity.

F. Percentages of heterodimers and each of the two homodimers for each of the 104 tested structures

20

when simulations consider differences in specific activity between homo- and heterodimers. The two homodimers were distinguished based on their abundance, such that high HM referred to the one with the higher concentration and low HM to the one with a lower concentration.

We then tested the effect of allowing different specific activities for homo- and heterodimers in our simulations of evolution. Our parametric simulations show that differences in specific activity can overturn the bias toward heterodimers when the optimum is set to 80 h^{-1} (Figure 5E, Figure S14). We observed a similar pattern in our simulations with structures (Figure 5F). Large differences in specific activity lead to 100% homodimers or 100% heterodimers, depending on the complex with higher specific activity. However, when these differences became very small, the system seemed slightly less efficient at eliminating the heterodimers. When the heterodimer was 10% less active than the homodimer, many structures still maintained a small fraction of heterodimers, whereas homodimers were essentially eliminated when the heterodimer was 10% more active. Interestingly, moving the optimal total activity from 80 h^{-1} to 60 h^{-1} led to important changes in the fitness landscape (Figure S15A) that altered drastically the results of the parametric simulations (Figure S15B). Whereas extreme biases in specific activity predictably led to the corresponding enrichment of homodimers or heterodimers depending on the more active dimer, HET activity values between -20% and 20% yielded more complex patterns. In this range of HET activity bias values, the simulations can approach the optimum activity value of 60 h^{-1} either by keeping a low total concentration of highly active complexes or by keeping a high total concentration of less active complexes, with the likelihood of each scenario depending on the distribution of mutational effects. Indeed, we saw both scenarios in our simulations with single structures (Figure S15C). However, when looking at the global trends for our simulations with structures the heteromer was still enriched even when it was around 20% less active than the homodimers (Figure S15D) since their distributions have more destabilizing effects on the homomers (see white triangle in Figure 2B) and slight mutational biases favoring the heterodimer (Figure 3). Thus, differences in specific activity can easily revert the bias toward heterodimers, but the most likely outcome would still be affected by the underlying distribution of mutational effects and the fitness function.

21

Discussion

There are many potential fates for duplicate genes. These often involve divergence of the paralogs in terms of function, regulation, and interactions with other proteins (Conant & Wolfe, 2008). Much work has been dedicated to describing the different outcomes (Hochberg *et al*, 2018; Marchant *et al*, 2019; Mallik & Tawfik, 2020) and developing models of the fate of duplicate genes (Force *et al*, 1999; Lynch & Conery, 2000; Gout & Lynch, 2015; Johri *et al*, 2022). However, we lack a thorough understanding of the underlying molecular determinants and evolutionary forces. The way mutations themselves can drive evolution through their biases towards specific phenotypic outcomes could play a role. For instance, subfunctionalization is more likely to occur than neofunctionalization because loss-of-function mutations are more likely than beneficial gains of function (Lynch & Force, 2000; Gibson & Goldberg, 2009). This alone could naturally bias the maintenance of gene duplicates in one direction even in the absence of natural selection favoring one outcome or the other. Here, we examine a special case of subfunctionalization which is the potential replacement of a homodimer by a heterodimer following gene duplication.

We characterized the equilibrium between homo- and heterodimers after duplication. Small effects on binding affinity in the range of 0.5 - 1 kcal / mol can drastically alter the proportions of homo- and heterodimers. Since our estimations of the distributions of mutational effects are centered close to that range (averages of 0.2 kcal / mol for heterodimers and 0.4 for homodimers), mutations that could shift the equilibrium are likely to be sampled often by evolution. Furthermore, although mutational effects on binding for homomers and heteromers are highly correlated, our FoldX predictions suggest that there is a small percentage of mutations that could directly stabilize one complex while destabilizing the other (Figure 3A, Figure S3A). Our model shows that changes in the proportion of the three complexes could therefore arise through a few mutations, matching previous reports of homomer evolution (Ashenberg *et al*, 2011; Garcia-Seisdedos *et al*, 2017; Hochberg *et al*, 2018) as well as heteromer evolution (Stutz & Blein, 2020; Emlaw *et al*, 2021).

In our simulated evolutionary trajectories, we observe that the most common outcome is for the proportion of heterodimers to increase. This result extends our previous observation that heterodimers of paralogs are often retained when only the homodimers are selected for (Marchant *et al*, 2019). However, a key difference is that in our previous study we considered selection acting on the ΔG_{bind} of one of the complexes, whereas here we consider selection acting on the total activity of the system. As such, the relative concentrations of homo- and heterodimers are allowed to drift as long as the total activity is maintained. The main implication of our results is that heterodimers of paralogs are likely to become the major functional unit over the ancestral homodimeric protein unless there is selection for the homodimer or against the heterodimer. Our conclusions are striking, especially when considering that interactions between identical chains (i.e., homodimers) are more likely to sample highly favorable binding energies when compared to interactions between different chains (i.e., heterodimers) (Lukatsky

22

634 *et al*, 2007; André *et al*, 2008). However, the same authors also identified that real structures of
635 superfamily heterodimers tend to have more favorable contacts between charged residues than
636 homodimers (Lukatsky *et al*, 2007). The mutational biases we observe would have a similar
637 effect in our simulations to such increases in favorable interactions, even though the increase in
638 the concentration of heterodimers was not explicitly selected for. Interestingly, others have
639 reported that symmetric assemblies tend to dominate over asymmetric ones (André *et al*, 2008).
640 In the case of heteromers of paralogs, they inherit the global structural symmetry of their
641 ancestral homomers because they come from a gene duplication. However, because the
642 subunits of the heterodimer of paralogs are encoded by different genes, they allow for local
643 differences in sequence that can provide more favorable contacts. Overall, the dominance of
644 heteromers in our simulations is in agreement with previous analyses of the homo and
645 heteromeric fates of paralogs in high-throughput PPI data (Mallik & Tawfik, 2020). However,
646 high-throughput PPI data are typically derived without considering barriers against
647 heteromerization (such as differential compartmentalization and expression) and the relative
648 abundance of each interaction. As such, further experimental characterization of the fates of
649 paralogs would require methods that address these issues.

650 The case for selection against heteromers might differ among protein families. For example,
651 selection against heteromers of paralogs has been pointed out as a way to reduce cross-talk
652 and promote specialization of transcription factors (Amoutzias *et al*, 2008), kinases (Ashenberg
653 *et al*, 2011), and chaperones (Pareek *et al*, 2011). However, differences in specificity in
654 transcription factors can also be achieved if one of the homomers and the heteromer are
655 retained (Mamnun *et al*, 2002; Baker *et al*, 2013). Others have reported positive selection for
656 heteromerization of transcription factors (Hernández-Hernández *et al*, 2007), as well as
657 allosteric (Kafková *et al*, 2017) and cooperative (Pillai *et al*, 2020) contributions of
658 heteromerization, which would act to preserve the heteromer. Interestingly, Pils and Schulz
659 (2004) have suggested that catalytically inactive protein domains are common (between 10%
660 and 15%) in eukaryotic proteomes. These catalytically inactive proteins are often conserved and
661 seem to have evolved regulatory functions mediated by binding to their paralogs (Pils & Schultz,
662 2004; Adrain & Freeman, 2012), providing a niche to preserve these heteromers. A final
663 consideration about the difficulty of removing heteromers is that the starting concentrations
664 immediately after duplication become more skewed towards heteromers as the number of
665 subunits in the oligomer increases. Because of this skew, higher order complexes require a
666 greater difference in the binding affinities of homomers and heteromers to promote specificity for
667 homomerization (Hochberg *et al*, 2018). Thus, it is unclear whether there would be selection
668 against most heteromers of paralogs and if it could be efficient enough to eliminate them.

669 Our results add to a growing body of work suggesting that complexity can increase neutrally
670 (Stoltzfus, 1999; Lynch, 2007; Hochberg *et al*, 2020; Muñoz-Gómez *et al*, 2021; Schulz *et al*,
671 2022; Abrusán & Foguet, 2023). In the case of heteromers of paralogs, two proteins would
672 become necessary to provide the function of an ancestral homomeric protein. Such transitions
673 increase the complexity of protein interaction networks, and they do not necessarily provide an
674 immediate adaptive benefit. A feature that can only be introduced by heteromers is mutational
675 asymmetry, which allows distinct sequences for the different subunits. Mutants that would

676 otherwise eliminate catalytic activity in a homomeric assembly can participate in heteromers
677 with native-like activity (Ebert *et al*, 2015). Indeed, the distributions we obtained when simulating
678 mutational effects *in silico* had smaller effects on heterodimers than on homodimers and often
679 had small enrichments in heterodimer-favoring mutations (Figure 3E-F). As a result, their
680 fixation could be a case of "survival of the flattest" due to smaller effects of point mutations
681 (Wilke *et al*, 2001). However, this comes with increases in network complexity that do not
682 contribute to robustness (Diss *et al*, 2017; Dandage & Landry, 2019). Overall, non-adaptive
683 processes play a significant role in the abundance of heteromers of paralogs in extant protein
684 interaction networks, although there are known examples of heteromers that provide an
685 adaptive benefit (Bridgham *et al*, 2008; Pillai *et al*, 2020).

686 Importantly, our model makes multiple simplifying assumptions. In order to keep the simulations
687 scalable, the distribution of mutational effects on folding free energy and binding affinity is kept
688 constant throughout, instead of being recalculated at every step. We make this assumption also
689 because while it is well-known that the effects of each new mutation are contingent on previous
690 mutations, whether the overall shape of the distribution stays the same is unclear. Similarly, any
691 systematic errors in our FoldX predictions would propagate as we simulate more mutations,
692 making the estimations progressively less accurate. However, given that we consider the
693 heterogeneity of the effects of mutations among the starting complexes, it is likely correct to
694 assume that the distribution of effects of mutations through time is captured in this initial
695 heterogeneity. Finally, our main conclusion about the likelihood of heterodimers to become more
696 abundant than homodimers depends on the shapes of the FoldX-derived distributions of
697 mutational effects. As shown in Figure 2B, modifying these distributions would lead to different
698 results. Thus, generating experimental data about how mutations affect the binding affinities of
699 homodimers and heterodimers of paralogs could help address this limitation.

700 We do not consider the potential effects of other covariates that would prevent interactions
701 between paralogs, such as compartmentalization (Marchant *et al*, 2019) and cotranslational
702 assembly (Shiber *et al*, 2018; Badonyi & Marsh, 2023). In these cases, the interaction between
703 the two paralogs would not be possible, and the system would be expected to preserve the
704 homomers. Our model also does not consider that tight binding could provide cross-stabilizing
705 contributions to protein folding, such as the ones modeled in Rotem et al. (2018), although the
706 fraction of properly folded subunits in our simulations consistently stays above 90% in most of
707 our simulations. Finally, as mutations accumulate, one might expect the specific activity of
708 homomers and heteromers to evolve. However, the distribution of mutational effects on specific
709 activity would be unique for each protein and without more knowledge on the distribution of
710 mutational effects on specific functions, we could make arbitrary choices that could bring the
711 balance in one direction or another. Relaxing our assumptions and including more cases would
712 allow our model to more accurately represent the fate of the paralogs, but our model already
713 shows the complex interplay between synthesis rates, folding energies, binding affinity, and
714 specific activities.

715 Our results highlight the importance of exploring neutral hypotheses for the evolution of
716 molecular systems. While clearly natural selection plays a role in shaping them, there appears

to be an important role of neutral evolution and mutational biases as well. Our result that heteromers of paralogs are likely to replace ancestral homomers after duplication agrees with recent observations that heteromers are more abundant in eukaryotic proteomes than in prokaryotes (Mallik & Tawfik, 2020; Schweke *et al*, 2023). This is consistent with the higher population sizes of prokaryotes (Lynch, 2006; Charlesworth, 2009), since any kind of selection against heteromers would be more efficient in these species than in eukaryotes. Future work should continue to investigate the factors leading to the fate of paralogs, focusing on how both natural selection and neutral evolution have contributed to the modern levels of complexity of protein interaction networks.

Materials and Methods

1.- Protein structures

1.1.- Selection of protein structures

The complete set of structures deposited on the Protein Data Bank (PDB) (Berman *et al*, 2000) were downloaded on March 29th, 2021. Structures were then filtered based on the following criteria:

- Experimental data: X-ray crystallography
- Author-assigned biological assembly: Dimeric
- Structures must have two identical subunits (no missing residues or both subunits miss the same residues)
- Sequence length was restricted to 60 - 450 residues

We mapped the remaining set of structures to their ECOD architecture annotations (Cheng *et al*, 2014). We selected structures from the major architecture types such that we had at least 7 of each one. Our final set comprised 104 PDB structures. These structures were clustered with CD-Hit version 4.8.1 (Li & Godzik, 2006; Fu *et al*, 2012) with the following parameters: -n 2 (word size), -c 0.4 (sequence identity threshold), -G 1 (global alignment), and -s 0.8 (length difference cutoff). All of our selected structures were identified in different clusters, confirming low sequence identity between them.

1.2.- Structural analyses

We studied different structural parameters for each protein structure (Figure S7). Secondary structures were annotated with DSSP version 2.2.1 (Kabsch & Sander, 1983). Interfaces were identified following Tsai et al. (1996). Residues were considered to be at the interface core if the distance between one of their non-hydrogen atoms and a non-hydrogen atom from any residue of the other subunit was smaller than the sum of their van der Waals radii plus 0.5 Angstroms. Residues within 6 Angstroms of the interface core but not in contact with the other subunit were classified as the interface rim. We analyzed the proportion of residues in contact with their counterparts from the other subunit as a proxy for symmetry at the interface. For this analysis,

753 we used a cut-off distance of 4 Angstroms between any non-hydrogen atoms of the two
754 residues on the two chains.

755 **2.- Estimation of distribution of mutational effects with FoldX**

756 The biological assemblies of selected PDB structures were generated using custom scripts
757 (Marchant *et al*, 2019). Energy minimization was performed on the biological assemblies using
758 the FoldX Repair function (Delgado *et al*, 2019) 10 times to ensure convergence (Usmanova *et*
759 *al*, 2018). Repaired structures were then used to perform *in silico* mutagenesis using the FoldX
760 BuildModel and AnalyseComplex functions (Delgado *et al*, 2019) with the MutateX workflow
761 (Tiberti *et al*, 2022) to estimate mutational effects on binding affinity and folding free energy.
762 Mutations were simulated in two runs for each complex: one run in which mutations were
763 applied on both subunits (simulating mutational effects for homomers) and one run in which
764 mutations were applied on only one subunit (simulating mutational effects for heteromers).
765 Mutational effects on binding affinity were taken from the corresponding distributions, while
766 mutational effects on folding free energy were taken from the distribution of effects on the
767 heteromer since our model uses changes on folding free energy to calculate the fraction of
768 properly folded subunits available for complex assembly.

769 **3.- Framework for simulations**

770 *3.1.- Pre-duplication model*

771 Our simulations consider a system of a gene encoding a protein (A) that forms a homodimer
772 (AA). Protein copies are synthesized with synthesis rate s_A and typical values for starting
773 parameters of folding free energy (ΔG_{fold} = -5 kcal / mol) (Pace, 1975; Plaxco *et al*, 2000) and
774 binding affinity (ΔG_{bind} = -10 kcal / mol) (Choi *et al*, 2015; Jankauskaitė *et al*, 2018). The
775 proportion of properly folded subunits is calculated based on equation 1 (Sailer & Harms, 2017):

776 $$w = \frac{1}{1+e^{\Delta G_{fold}}} \qquad (1)$$

777 where w is the fraction of folded proteins and ΔG_{fold} is the free energy of the native fold.

778 Properly folded subunits are considered for the formation of complexes while the remaining
779 misfolded subunits are removed (assumed to be degraded/not to participate in the formation of
780 complexes). Decay rates for properly folded monomers (d_A) and homodimers (d_{AA}) are set to 1.3
781 h^{-1}, following the derivation by Hausser et al (2019) based on median protein half-life and cell
782 division rate for yeast. The assembly of homodimers is driven by the association constant k_{AA}.
783 Thus, using s_A, w, d_A, d_{AA}, and k_{AA} we can calculate the expected concentrations at equilibrium
784 of A and AA (see full derivation in Supplementary File 1). The equilibrium concentrations of
785 monomers and homodimers are multiplied by their specific activity (0.1 for monomers, 1 for the
786 homodimer) to calculate the total activity of the system. Fitness is determined from a lognormal
787 function (defined by alpha and beta parameters) from the total activity of the system. Since the

total activity before duplication was calculated at 38.2 h^{-1}, the optimum fitness was set at 60 h^{-1} or 80 h^{-1} (alpha parameter) to favor duplication events. The beta parameter was set to 0.5 so that fitness would be reduced by half when the total activity was either half or twice the alpha parameter.

At the start of the simulation, each mutation has a probability of being a mutation on the coding sequence, a duplication, or a mutation causing a change in synthesis rate. The effects of coding mutations on folding free energy ($\Delta\Delta G_{fold}$) and binding affinity ($\Delta\Delta G_{bind}$) are sampled from distributions of mutational effects (see section 3.3) and are used to calculate the fraction of properly folded subunits and the equilibrium constants, respectively. Equation 2 shows how the association constants for each dimer are calculated once ΔG_{bind} is updated with the effect of the sampled mutations ($\Delta\Delta G_{bind}$):

$$K_{AA} = e^{\frac{-(\Delta G_{bind,AA} + \Delta\Delta G_{bind,AA})}{RT}} \qquad (2)$$

where R is the gas constant (1.987 x 10^{-3} cal K^{-1} mol^{-1}) and T is temperature at 298 K. Once a mutation has been sampled, the equilibrium concentrations of all molecular species and the total activity of the system are recalculated using equations 3 and 4 (full derivation in Supplementary File 1):

$$c_A = \frac{-d_A + \sqrt{d_A^2 + 8\, d_{AA}\, k_{AA}\, s_A}}{4\, d_{AA}\, k_{AA}} \qquad (3)$$

$$c_{AA} = k_{AA}\, c_A^2 \qquad (4)$$

where c_A and the c_{AA} are the concentrations of each molecular species, d_A and d_{AA} are the decay rates of each molecular species, s_A is the rate of synthesis of properly folded subunits of A, and k_{AA} is the association constant for AA.

Using the new equilibrium concentrations, the fitness of the new state is compared to that of the previous state. Simulations continue until 200 mutations have been fixed, with the first one being the duplication. Duplications introduce new molecular species: monomer B, homodimer BB, and heterodimer AB. As a result, the calculations for the equilibrium concentration of each complex change (see next section).

3.2.- Post-duplication system

Once a duplication has been fixed, the system will have two genes encoding two proteins (A and B) that will assemble into complexes AA, AB, and BB. Mutations continue to be sampled from the underlying distribution of mutational effects, and the system no longer samples for further duplication events. Once a mutational effect is selected, the affected protein (A or B) is selected at random. Afterwards, the new ΔG_{fold} is calculated to estimate the fraction of properly

folded subunits and the ΔG_{bind} for both the homodimeric and heterodimeric interactions are used to estimate the new equilibrium constants. Following Hochberg et al. (2018), a factor of 2 is used to correct for the mixing entropy difference that inherently favors heteromers in the mixture of heterodimers and homodimers. Once all the values are calculated, the 4th degree polynomial in equation 5 is used to estimate the concentration at equilibrium of A (full derivation in Supplementary File 2):

$$\begin{gathered}
0 \\
= \\
2 d_{AA} k_{AA} \left(4 \frac{d_{AA} k_{AA} d_{BB} k_{BB}}{d_{AB} k_{AB}} - d_{AB} k_{AB} \right) c_A^4 \\
+ \\
\left(d_A \left(8 \frac{d_{AA} k_{AA} d_{BB} k_{BB}}{d_{AB} k_{AB}} - d_{AB} k_{AB} \right) - 2 d_B d_{AA} k_{AA} \right) c_A^3 \\
+ \\
\left(\frac{2 d_{BB} k_{BB} d_A^2}{d_{AB} k_{AB}} + s_A \left(d_{AB} k_{AB} - 8 \frac{d_{AA} k_{AA} d_{BB} k_{BB}}{d_{AB} k_{AB}} \right) - d_A d_B - d_{AB} k_{AB} s_B \right) c_A^2 \\
+ \\
s_A \left(d_B - 4 d_A \frac{d_{BB} k_{BB}}{d_{AB} k_{AB}} \right) c_A \\
+ \\
2 s_A^2 \frac{d_{BB} k_{BB}}{d_{AB} k_{AB}}
\end{gathered} \tag{5}$$

where *dA*, *dB*, *dAA*, *dAB*, and *dBB* are decay rates for each molecular species; *sA* and *sB* are the synthesis rates of properly folded subunits of A and B; *kAA*, *kAB*, and *kBB* are the association constants for each of the dimers.

Once the four potential solutions to the concentration of A are known, the concentrations of the rest of the molecular species are calculated using equations 6-9:

$$c_B = \frac{s_A / c_A - 2 d_{AA} k_{AA} c_A - d_A}{d_{AB} k_{AB}} \tag{6}$$

$$c_{AA} = k_{AA} c_A^2 = \frac{r_2}{d_{AA} + r_1} c_A^2 \tag{7}$$

$$c_{BB} = k_{BB} c_B^2 = \frac{r_4}{d_{BB} + r_3} c_B^2 \tag{8}$$

28

$$c_{AB} = k_{AB} c_A c_B = \frac{r_6}{d_{AB} + r_5} c_A c_B \qquad (9)$$

where r_1, r_3, and r_5 are dissociation rates of AA, BB, and AB, respectively; r_2, r_4, and r_6 are association rates of AA, BB, and AB, respectively.

Among the four possible solutions to the complete system of equations, the physically correct solution is the one that results in positive values for the concentrations of all five molecular species.

3.3.- Parametric distributions of mutational effects

We performed simulations by sampling from multivariate normal distributions of mutational effects. Each multivariate normal distribution was used to sample effects on ΔG_{fold} for each monomer, $\Delta G_{bind, AA}$ for the homodimer, and $\Delta G_{bind, AB}$ for the heteromer. We set the means of the multivariate normal distributions and the correlations between variables to values similar to those observed in the distributions simulated with FoldX:

- Effects on ΔG_{fold}: N(2.6, 4.6)
- Effects on $\Delta G_{bind, AB}$: N(0.2, 1.2)
- Effects on $\Delta G_{bind, AA}$: The mean was allowed to vary between 0.06 and 0.6, while the standard deviation varied between 0.6 and 3 (Figure 2B). For all other figures showing results of simulations with parametric distributions, the standard deviation was kept constant at 2.4.
- Correlation between effects on ΔG_{fold} and $\Delta G_{bind, AB}$: 0.3
- Correlation between effects on ΔG_{fold} and $\Delta G_{bind, AA}$: 0.3
- Correlation between effects on $\Delta G_{bind, AA}$ and $\Delta G_{bind, AB}$: 0.9

3.4.- Simulations allowing changes in gene expression

A subset of the simulations were run allowing mutations to have an effect on gene expression. For each sampled mutation, a given probability (ranging from 0.1 to 0.9) was given that a mutation would have an effect on synthesis rates instead of the coding sequence. The underlying distribution of mutational effects on gene expression was based on a fit to previously published work on the TDH3 promoter (Metzger *et al*, 2016). The data were fit to a skew normal distribution, which gave the following parameters: mean = 0, standard deviation = 0.025, skew = -0.125. Since the mutational effects reported by Metzger et al. (2016) were normalized with respect to the WT, they were applied by multiplying the sampled values times the current synthesis rate.

3.5.- Simulations with biases in specific activity

A subset of the simulations were run to explore the outcomes when the homo- and heterodimers had different specific activities. To bias a simulation towards homodimers, the specific activity for

homodimers was kept at 1 while the specific activity of heteromers was given a value ranging from 0.1 to 0.9, and vice versa to bias simulations toward heterodimers.

4.- Data analysis

For each structure, we analyzed the results of 50 replicate simulations. Each replicate continued until 200 mutations were fixed. We tracked the equilibrium concentrations of all molecular species (monomers A and B; homodimers AA and AB; and heteromer BB) through time. We defined terms for the relative concentration of each molecular species at the end of the simulation according to equation 10:

$$p_X = \frac{100 * c_X}{c_A + c_B + c_{AA} + c_{AB} + c_{BB}} \qquad (10)$$

where *pX* indicates the relative concentration of X (X being any of A, B, AA, AB, or BB) and cX indicates the concentration of X.

We analyzed enrichments in homomers or heteromers by looking for deviations from the initial conditions post-duplication (25% AA, 50% AB, 25% BB). As such, replicates were classified based on the relative concentrations of each species at the end of the simulation:

- HET dominant: 70 <= pAB
- HM dominant: 70 <= (pAA + pBB)
- Both HM and HET: 70 <= (pAB + pAA + pBB) AND 70 >= pAB AND 70 >= (pAA + pBB)
- Monomers: 70 <= (pA + pB)
- Ambiguous: 70 >= (pAB + pAA + pBB) AND 70 >= (pA + pB)

Our measure for the results of the simulation was the concentration of each molecular species at the end, averaged over all replicates.

All scripts are available on Github (https://github.com/Landrylab/Homomer_duplication_2023) with supporting data on Zenodo (https://zenodo.org/records/10048861).

30

Attributions:

AFC, LNT, and CRL designed research. LNT derived the system of equations used in the model. LNT and AFC wrote the framework for simulations. AFC ran simulations and characterized the solution space for the system of equations. AFC, SM and CRL analyzed results. AFC and CRL wrote the paper with input from LNT and SM. EDL and CRL supervised research.

Acknowledgments:

We thank François Rouleau, Soham Dibyachintan, Adrian Serohijos, Sarah Otto, and members of the Landry and Levy labs for their feedback and help on the project. The computer cartoon used to denote parametric simulations was created by Jan Flessau.

Funding:

This work was supported by Canadian Institutes of Health Research (CIHR) Foundation grant 387697 (to C.R.L.), Canada Research Chair in Cellular Systems and Synthetic Biology (to C.R.L.), Fonds de recherche du Québec - Nature et technologies (FRQNT) Merit Scholarship Program for Foreign Studies (PBEEE) (to A.F.C.), joint funding from MEES and AMEXCID (to A.F.C.), Mitacs Globalink Research Award (to A.F.C.), Alexander Graham Bell fellowship from the National Sciences and Engineering Research Council of Canada (NSERC) (to L.N-T), FRQNT funding (to L.N-T), European Research Council (ERC) under the European Union's Horizon 2020 research and innovation program (grant agreement No. 819318, to E.D.L.), by the Israel Science Foundation grant no. 1452/18 (to E.D.L.), and by the Abisch-Frenkel Foundation (to E.D.L.).

Conflict of interest:

The authors declare no conflict of interest.

31

Supplementary Material

Supplementary File 1: Complete derivation of system of equations for pre-duplication equilibrium

Supplementary File 2: Complete derivation of system of equations for post-duplication equilibrium

32

Supplementary Figures

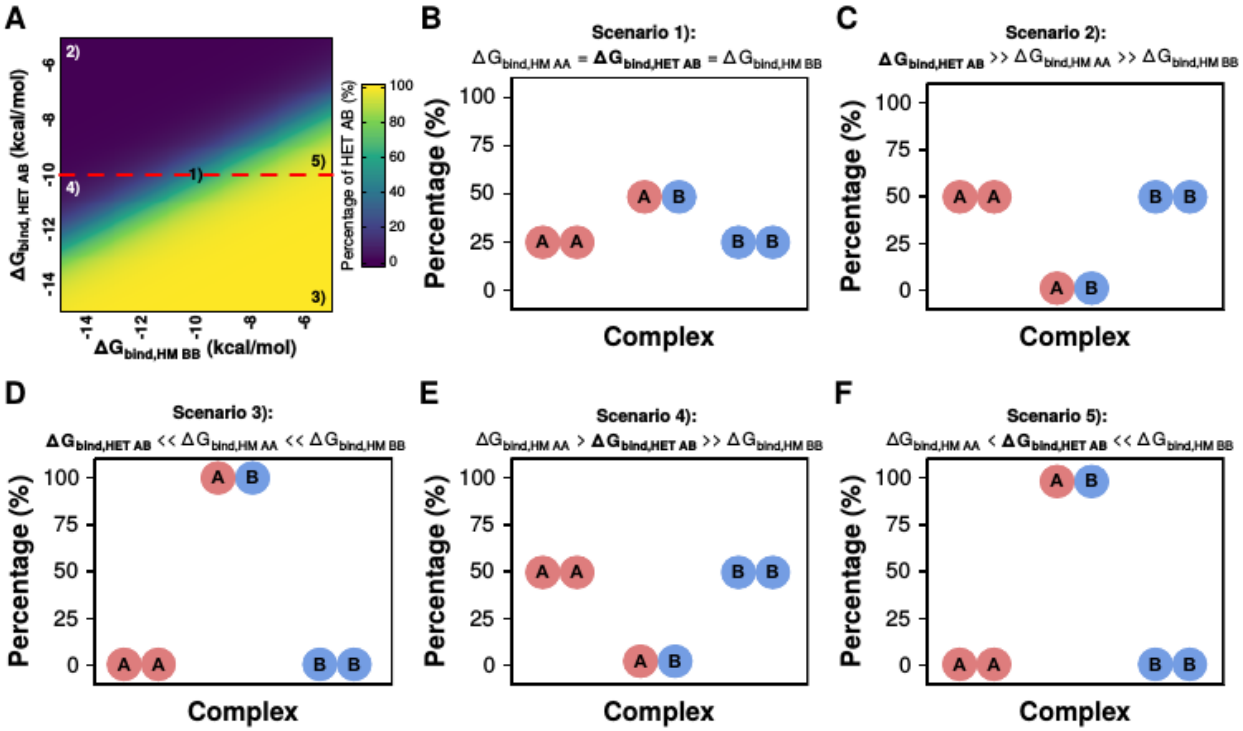

Figure S1. The equilibrium between homodimers and heterodimers is determined by binding affinities.

A. Effect of variation in $\Delta G_{bind,AB}$ and $\Delta G_{bind,BB}$ on the percentage of heterodimers, similar to Figure 1G. The dashed red line indicates the value of $\Delta G_{bind,AA}$, which is kept constant at -10 kcal/mol. Numbered labels inside the heatmap indicate the different scenarios described in the rest of the panels.

B. Scenario 1): Directly after the duplication, the binding affinities of the three dimers are identical, leading to a 25% AA:50% AB:25% BB equilibrium.

C. Scenario 2): Homomers dominate when the heterodimer has the weakest binding affinity.

D. Scenario 3): Heterodimers dominate when they have the strongest binding affinity.

E. Scenario 4): Homomers dominate when the binding affinity of the heterodimer is slightly stronger than that of one of the homodimers but much weaker than the other one.

F. Scenario 5): Heterodimers dominate when the binding affinity of the heterodimer is slightly weaker than that of one of the homodimers but much stronger than the other one.

33

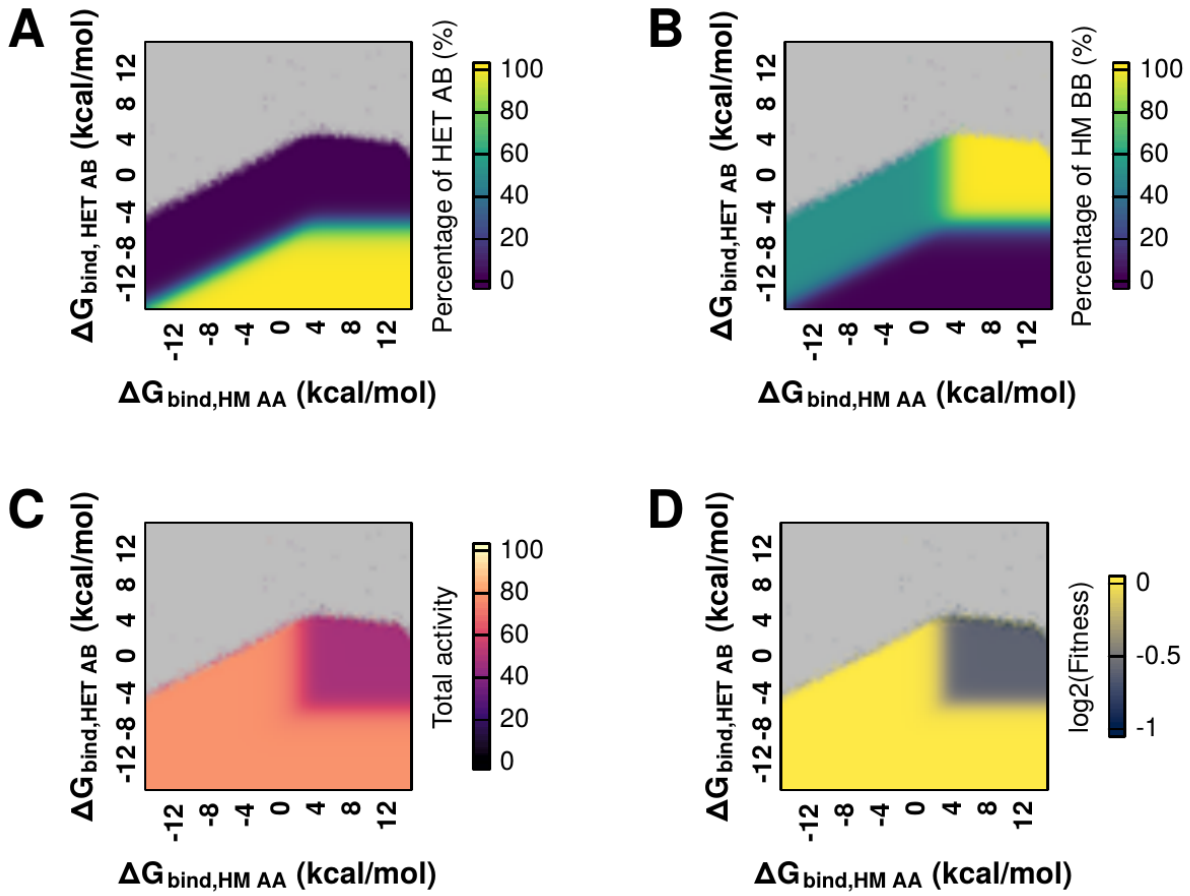

933 **Figure S2. Effects of an extended range of different values of binding affinity ($\Delta G_{bind,AB}$ and**
934 **$\Delta G_{bind,AA}$) on the equilibrium between homo- and heterodimers.**
935 **A-D.** Effect of variation in $\Delta G_{bind,HET\ AB}$ and $\Delta G_{bind,HM\ AA}$ on the percentage of the heterodimer (HET AB) (A),
936 percentage of one of the homodimers (HM AA) (B), and the total activity (C), and fitness (D) of the
937 system. For panels A-D, $\Delta G_{bind,HM\ BB}$ was kept constant at -10 kcal /mol. The space in grey at the top of
938 each heatmap represents the sets of values for which the equation solver could not find an equilibrium,
939 because the polynomial coefficients (proportional to $(k_{AA}^2 * k_{BB})/k_{AB}$, see equations 2 and 5 in Methods)
940 become too large.

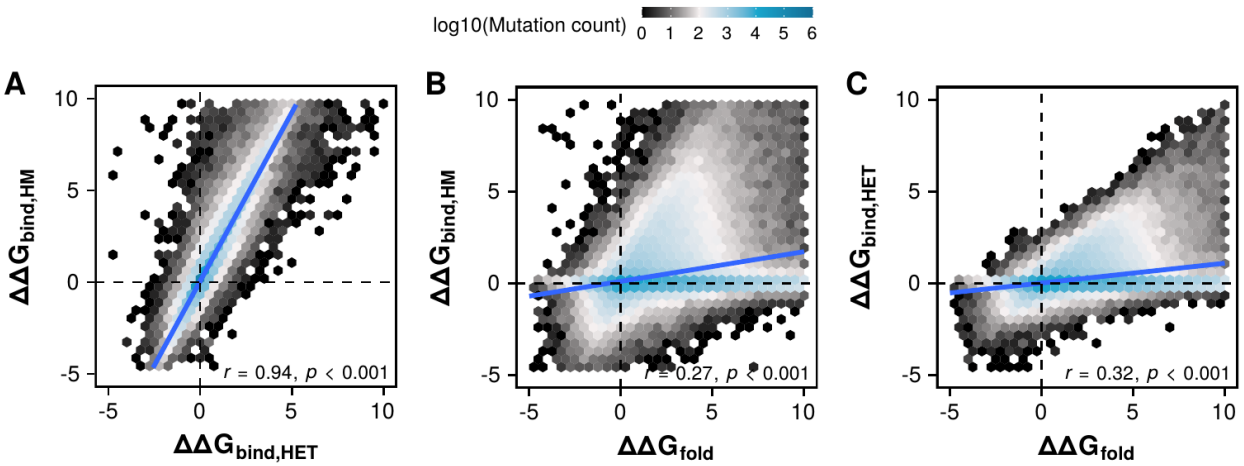

Figure S3. Bidimensional distributions of mutational effects on $\Delta G_{bind,HET}$, $\Delta G_{bind,HM}$, and ΔG_{fold}. **A-C**. Hexagonal bins indicate the density of mutational effects for the pool of mutations for all structures. Two variables and their correlations are shown in each panel: $\Delta G_{bind,HET}$ and $\Delta G_{bind,HM}$ (A), $\Delta G_{bind,HM}$ and ΔG_{fold} (B), $\Delta G_{bind,HET}$ and ΔG_{fold} (C).

35

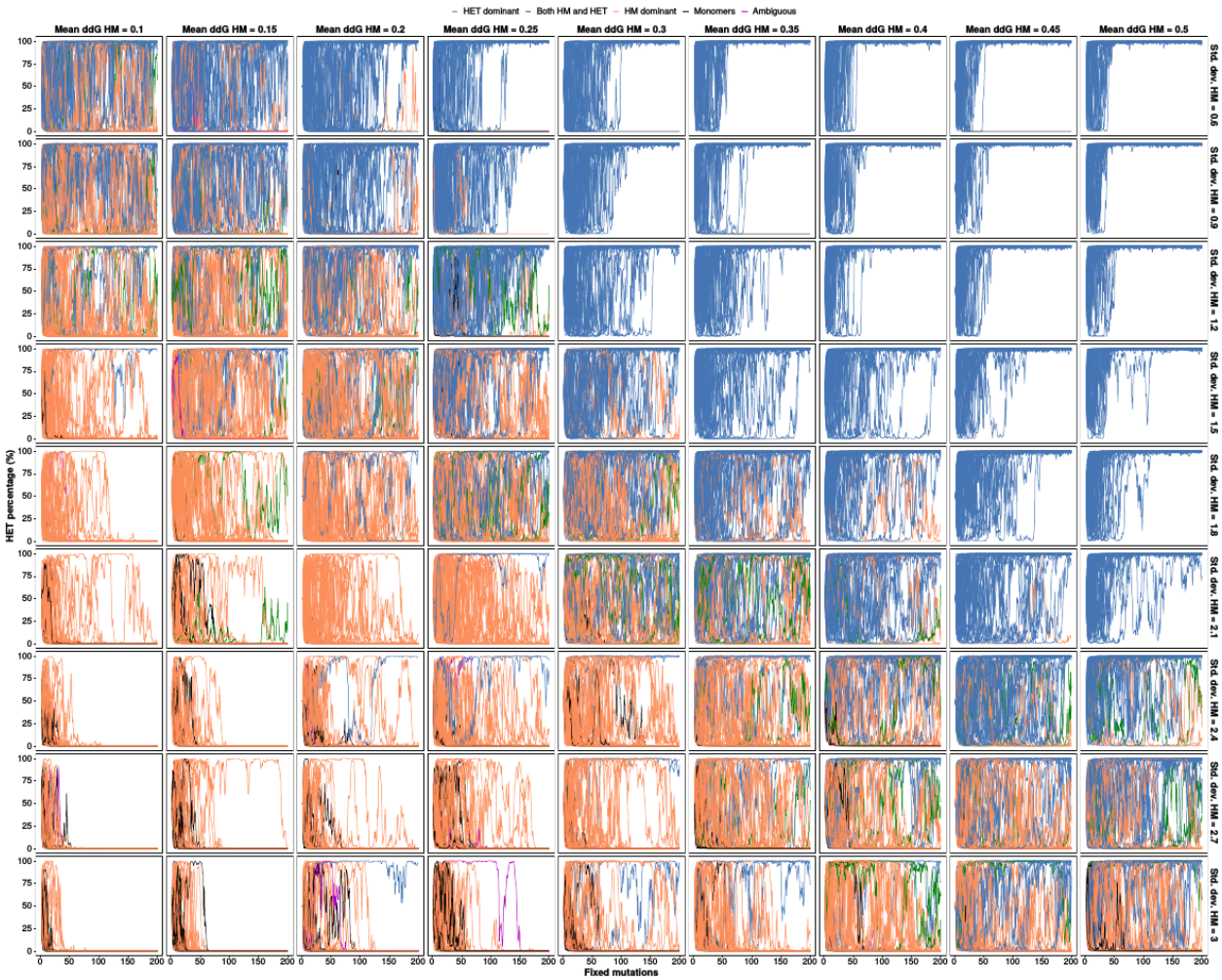

Figure S4. Trajectories of individual replicates of parametric simulations. Panels show trajectories of 50 individual replicates of parametric simulations with different means and standard deviations for the distribution of effects on $\Delta G_{bind,HM}$ (same data as in figure 2B). Replicates were colored according to the equilibrium concentrations of complexes at the end of each simulation following the classification outlined in section 4 of the methods: HET dominant: 70 <= pAB, HM dominant: 70 <= (pAA + pBB), both HM and HET: 70 <= (pAB + pAA + pBB) AND 70 >= pAB AND 70 >= (pAA + pBB), monomers: 70 <= (pA + pB), ambiguous: 70 >= (pAB + pAA + pBB) AND 70 >= (pA + pB)

36

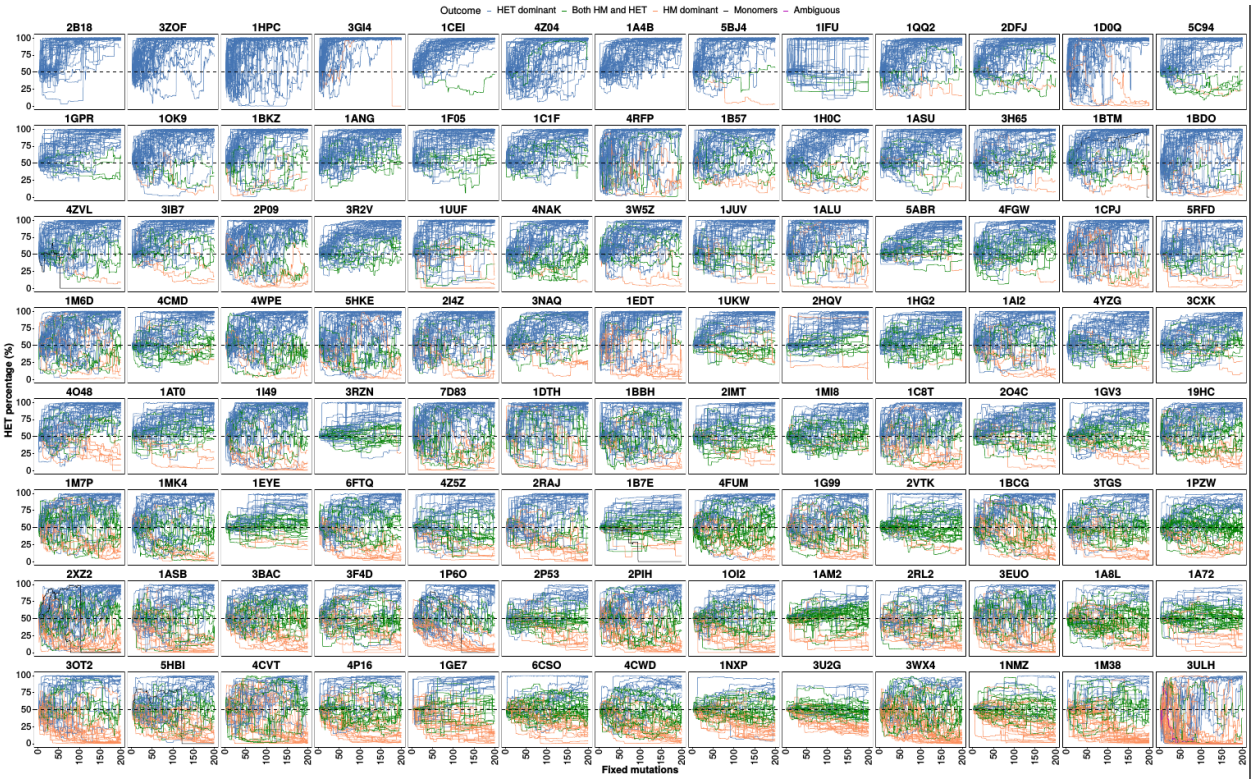

Figure S5. Trajectories of individual replicates of simulations with structures. Panels show trajectories of 50 individual replicates of simulations using the distributions of mutational effects estimated for each PDB structure (same data as in figure 2C). Replicates were colored according to the equilibrium concentrations of complexes at the end of each simulation following the classification outlined in section 4 of the methods: HET dominant: 70 <= pAB, HM dominant: 70 <= (pAA + pBB), both HM and HET: 70 <= (pAB + pAA + pBB) AND 70 >= pAB AND 70 >= (pAA + pBB), monomers: 70 <= (pA + pB), ambiguous: 70 >= (pAB + pAA + pBB) AND 70 >= (pA + pB)

37

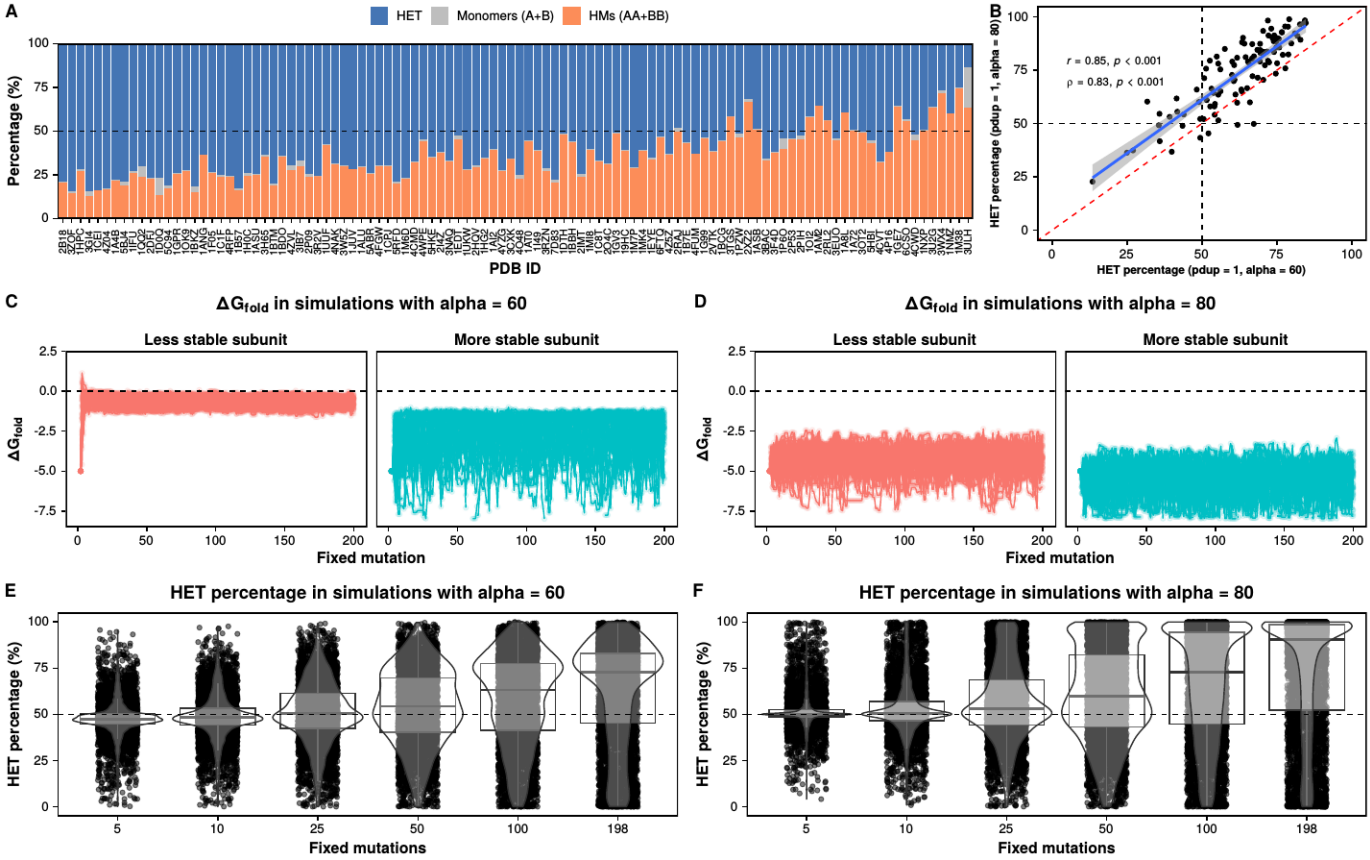

Figure S6. The general bias observed for heterodimers is also observed when the optimal activity is set to a slightly lower value (alpha = 60).

A. Percentage of heterodimers, homomers, and monomers at the end of simulations with distributions of mutational effects structures when the optimal activity (alpha) is set to 60. Structures are listed in the same order as in figure 2C.

B. Correlation between the percentages of heterodimers observed at the end of simulations with alpha = 60 (data from figure S6A) and simulations with alpha = 80 (data from figure 2C).

C-D. Evolution of ΔG_{fold} values in simulations with alpha = 60 (C) and alpha = 80 (D). For simplicity, only the data for PDB: 1GPR are shown.

E-F. Evolution of the percentage of heteromers in simulations with alpha = 60 (E) and alpha = 80 (F). Replicates for all simulations with all structures are shown.

38

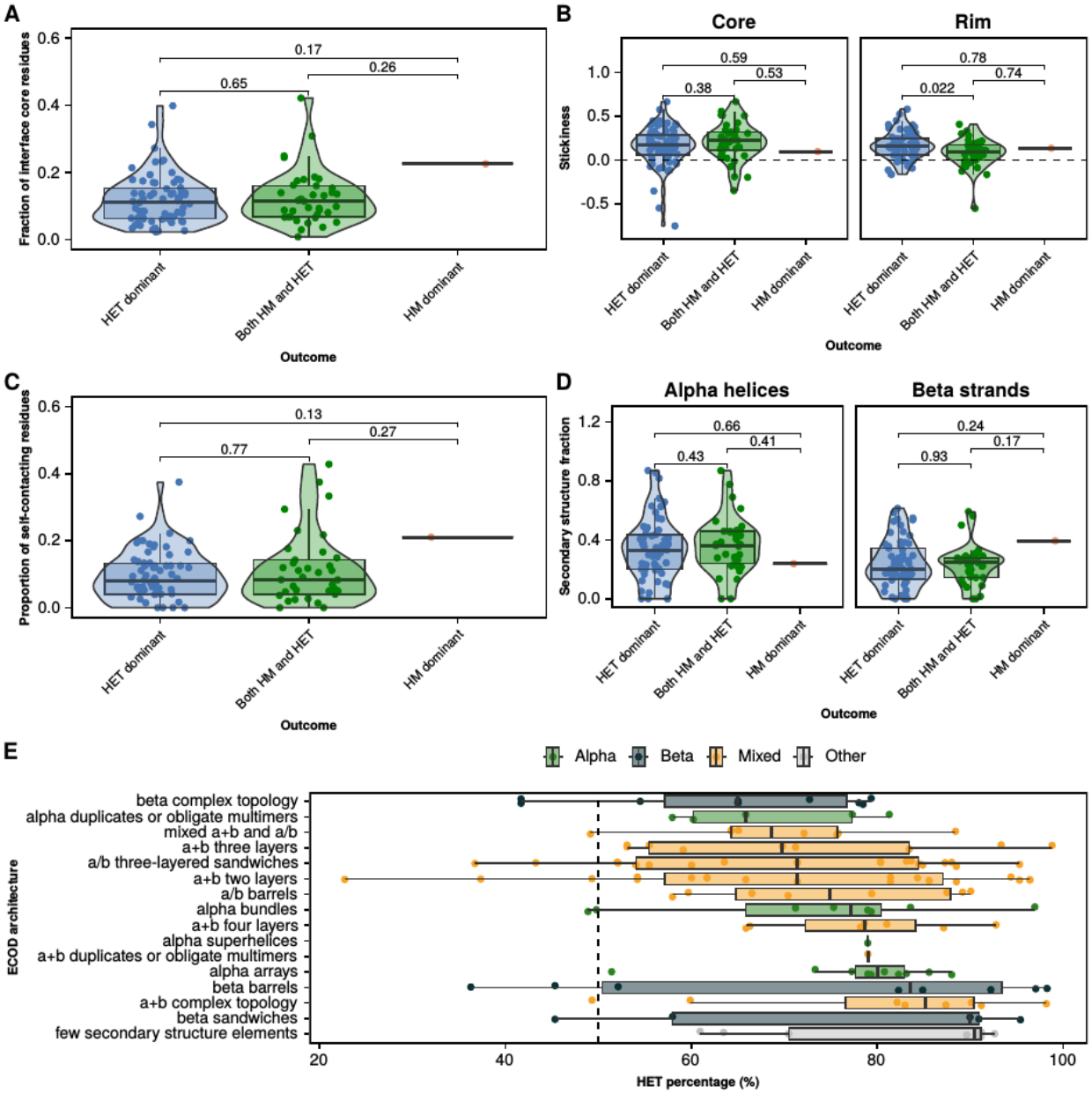

Figure S7. No clear effects of structural properties of protein interaction interfaces on the observed outcomes.

A-D. Distributions for all 104 structures tested for fraction of residues of the whole protein that are located in the interface core (A), the average stickiness of the interface core and rim (B), the proportion of residues in the interface core and rim that are within 4 Angstroms of their counterparts in the opposite subunit (C), and the percentage of alpha helices and beta strands at the interface (D). Structures were classified in panels A-D according to the outcome of their simulations from figure 3A. p-values were calculated using Wilcoxon tests.

E. Percentages of heteromers at the end of the simulation for dimers with different ECOD architectures. Architectures are classified according to their dominant secondary structure (alpha helices, beta strands, or mixed).

39

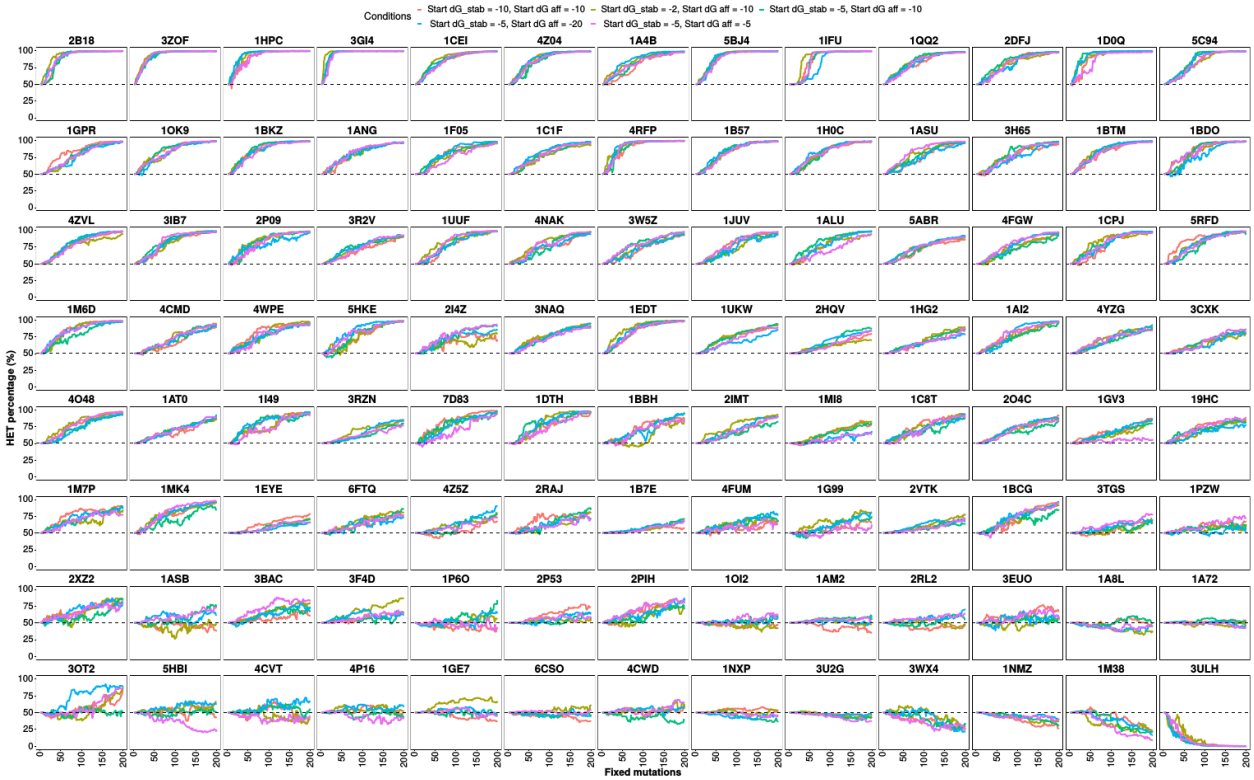

Figure S8. Changes in the starting values for ΔG_{fold} and ΔG_{bind} do not alter the outcome significantly. Simulations were run using the distributions of mutational effects for each PDB structure and changing the starting parameters for ΔG_{fold} and ΔG_{bind}. Each combination of values was selected by doubling or halving one of the reference parameters (ΔG_{fold} = -5 kcal/mol, ΔG_{bind} = -10 kcal/mol) while keeping the other one constant.

40

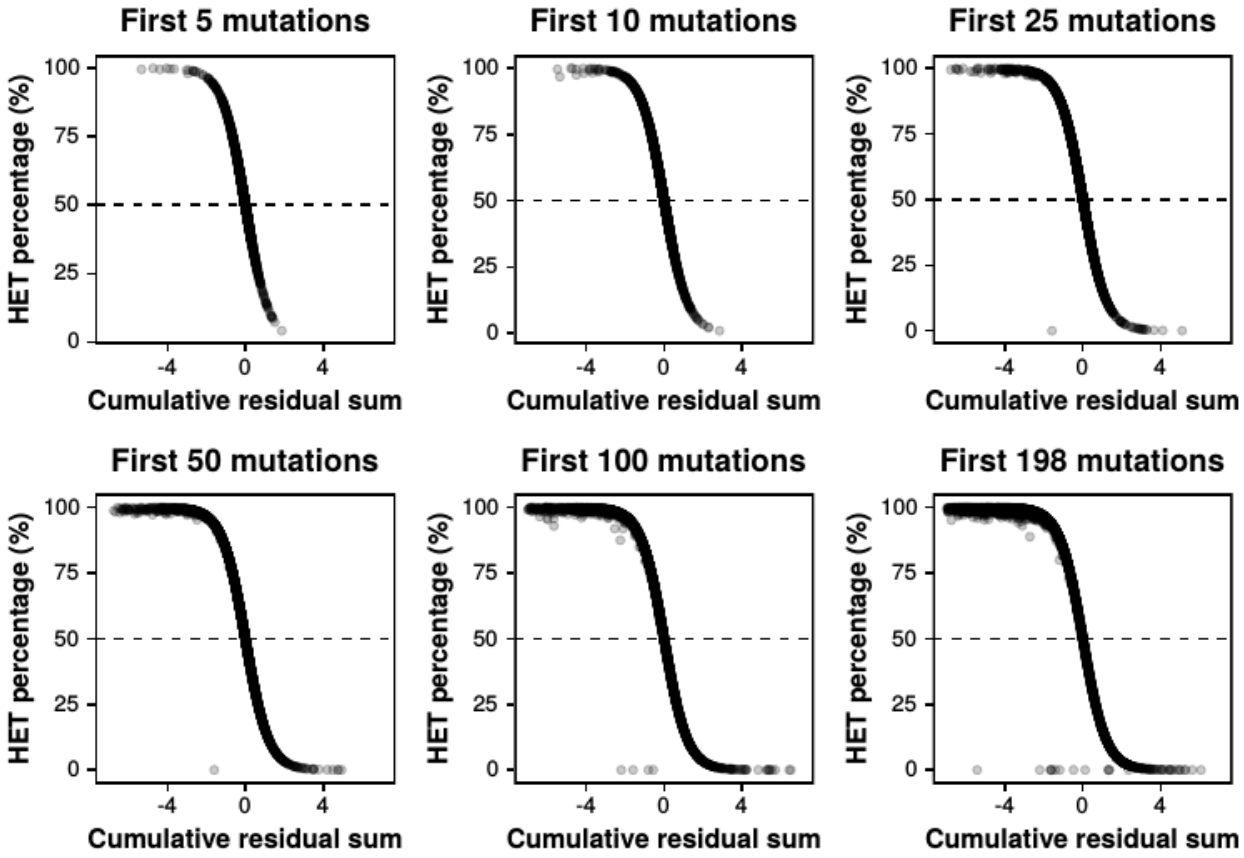

Figure S9. The cumulative sum of residuals of fixed mutations reflects the percentage of heteromers. For each replicate of simulations with each structure, the residuals of fixed mutations up to specific points in the simulation (5, 10, 25, 50, 100, 198 mutations) were added and compared to the percentage of heterodimers at that point in the simulation.

41

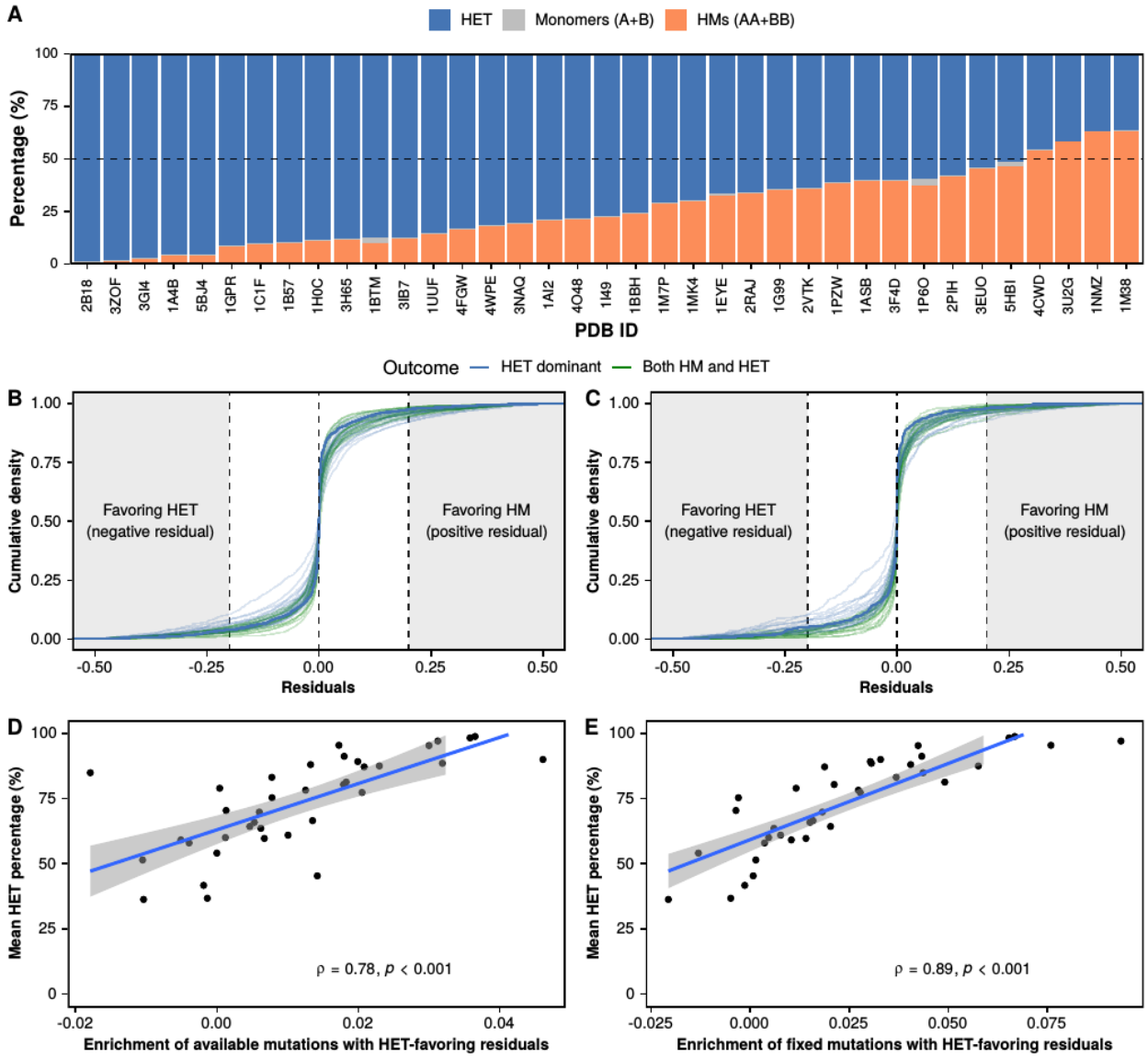

Figure S10. Mutational biases promote the enrichment of heterodimers in very high quality PDB structures.

A. Average percentages of heterodimers, homodimers, and monomers for each of the very high quality PDB structures at the end of the simulations. The dashed line indicates the starting point at 50% heterodimers and 50% homodimers (25% of each homodimer).

B-C. Distributions of available (B) and fixed (C) residuals with respect to the expectation for each of the 37 very high quality structures. Colors indicate mean outcomes for each structure: HET dominant (heterodimer > 70% of dimers), HM dominant (homodimer > 70% of dimers), both HM and HET (rest of cases). The thicker blue line represents 2B18. Shaded regions on the left and right indicate mutations whose residuals have a magnitude of at least 0.2 favoring either the heterodimer (negative values) or the homodimer (positive values).

D-E. Correlation between enrichment of available (D) and fixed (E) mutations with residuals favoring the heterodimer and the mean percentage of heterodimers at the end of the simulations. The enrichment of heterodimer-favoring residuals is calculated as the density of mutations with residuals smaller than -0.2 minus the density of mutations with residuals greater than 0.2.

42

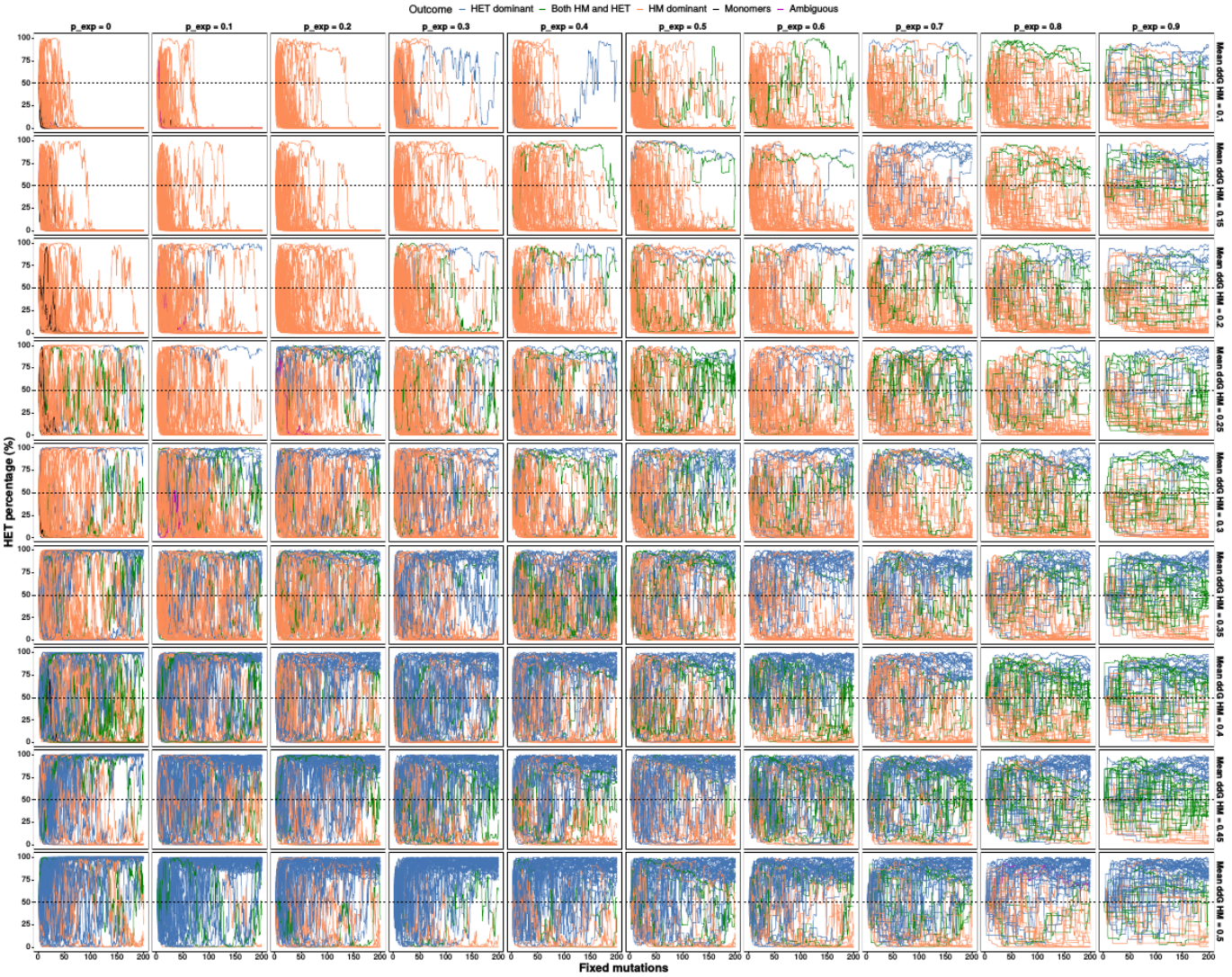

Figure S11. Trajectories of individual replicates for parametric simulations that allow changes in synthesis rates. Individual replicates were colored based on the percentage of heteromers at the end of the simulation following the classification outlined in section 4 of the methods: HET dominant: 70 <= pAB, HM dominant: 70 <= (pAA + pBB), both HM and HET: 70 <= (pAB + pAA + pBB) AND 70 >= pAB AND 70 >= (pAA + pBB), monomers: 70 <= (pA + pB), ambiguous: 70 >= (pAB + pAA + pBB) AND 70 >= (pA + pB). The data shown are the same as in figure 4E.

43

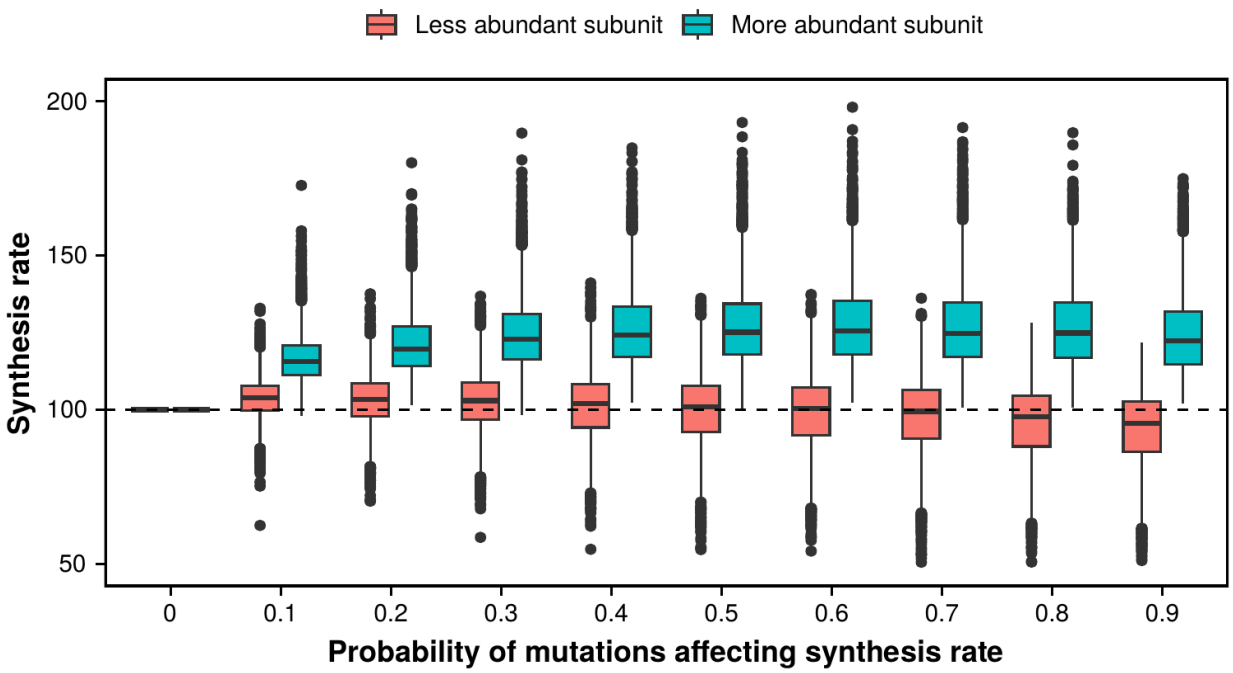

1012 **Figure S12. Divergence in synthesis rates between paralogs in simulations with structures.**
1013 Simulations were run using the distributions of mutational effects for all replicates of each of the 104 PDB
1014 structures and different probabilities of mutations affecting synthesis rates. For each simulation, the more
1015 abundant subunit and the least abundant subunit were distinguished. The dashed line at 100 indicates the
1016 starting synthesis rate for both subunits.

44

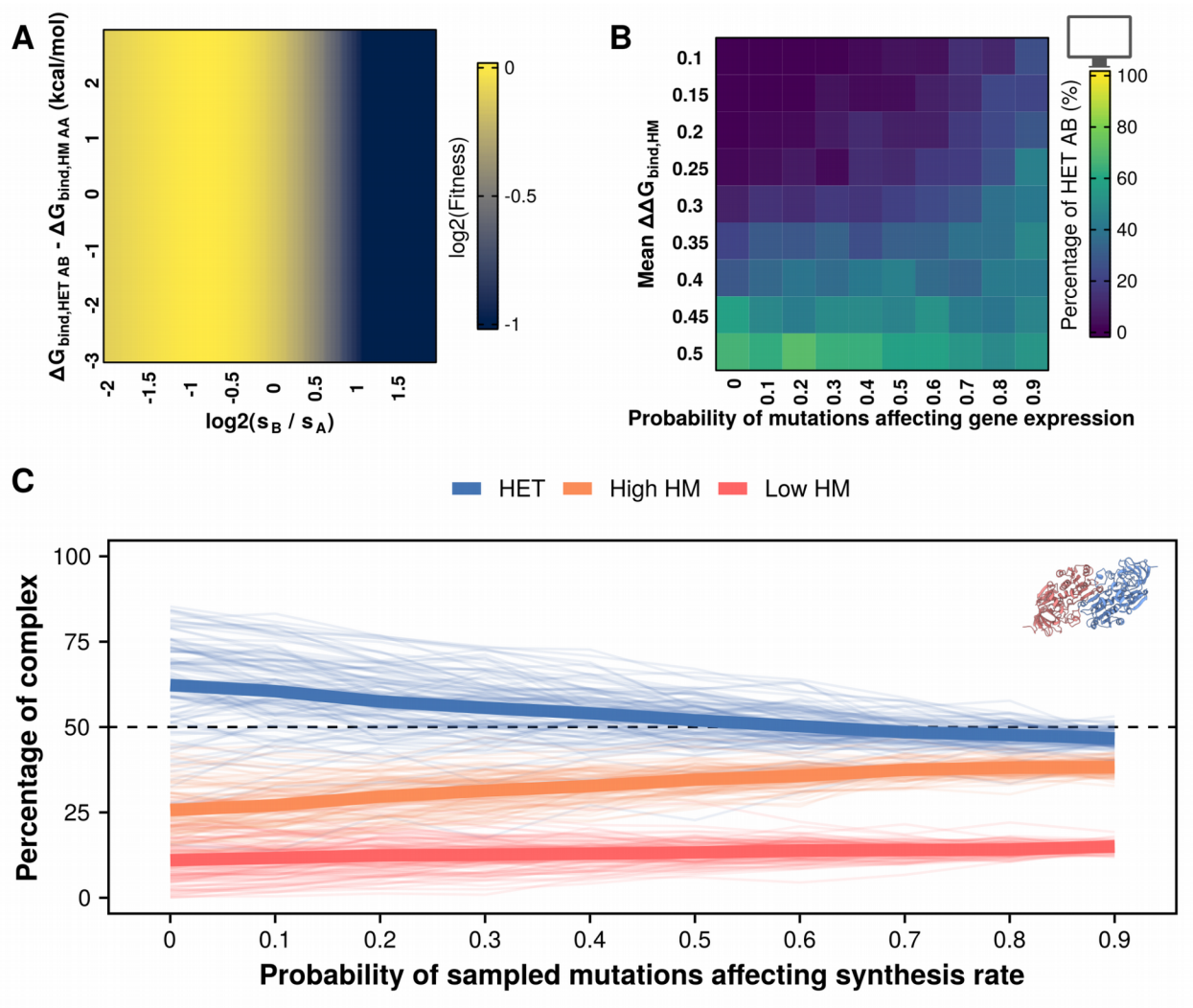

Figure S13. Simulations allowing changes in synthesis rates with lower optimal activity (alpha = 60).

A. Fitness landscape when the optimal activity is set to 60. Note that s_A, $\Delta\Delta G_{bind,AA}$, and $\Delta\Delta G_{bind,BB}$ remain constant throughout.

B. Percentages of heterodimers at the end of parametric simulations allowing changes in synthesis rates and varying mean effects of mutations on homodimers.

C. Percentages of heterodimers and each of the two homodimers for each of the 104 tested structures when simulations consider different probabilities of mutations affecting synthesis rates. The two homodimers were distinguished based on their abundance.

45

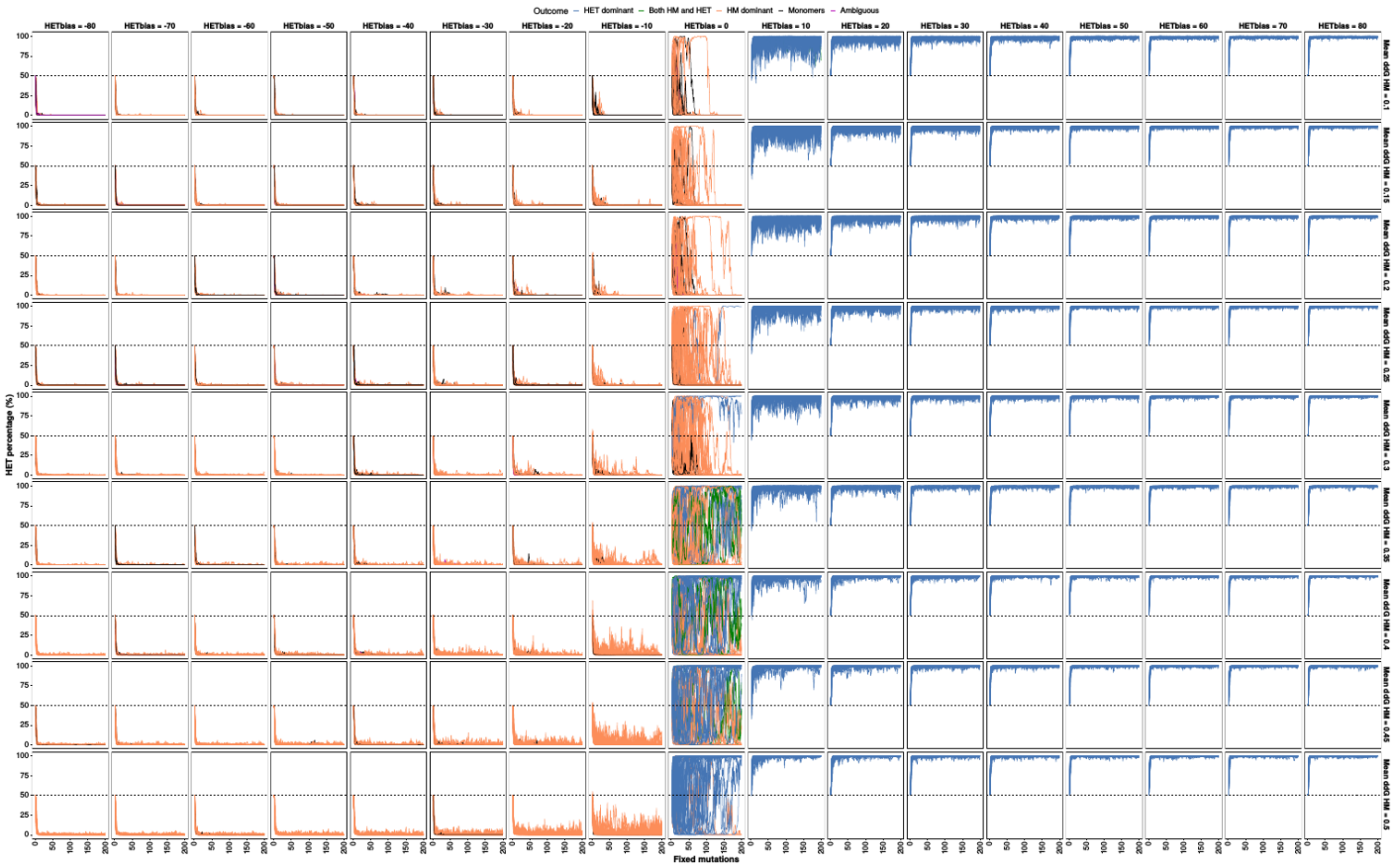

Figure S14. Individual trajectories for parametric simulations with differences in specific activities. Individual replicates were colored based on the percentage of heteromers at the end of the simulation following the classification outlined in section 4 of the methods: HET dominant: 70 <= pAB, HM dominant: 70 <= (pAA + pBB), both HM and HET: 70 <= (pAB + pAA + pBB) AND 70 >= pAB AND 70 >= (pAA + pBB), monomers: 70 <= (pA + pB), ambiguous: 70 >= (pAB + pAA + pBB) AND 70 >= (pA + pB). The data shown are the same as in figure 5E.

46

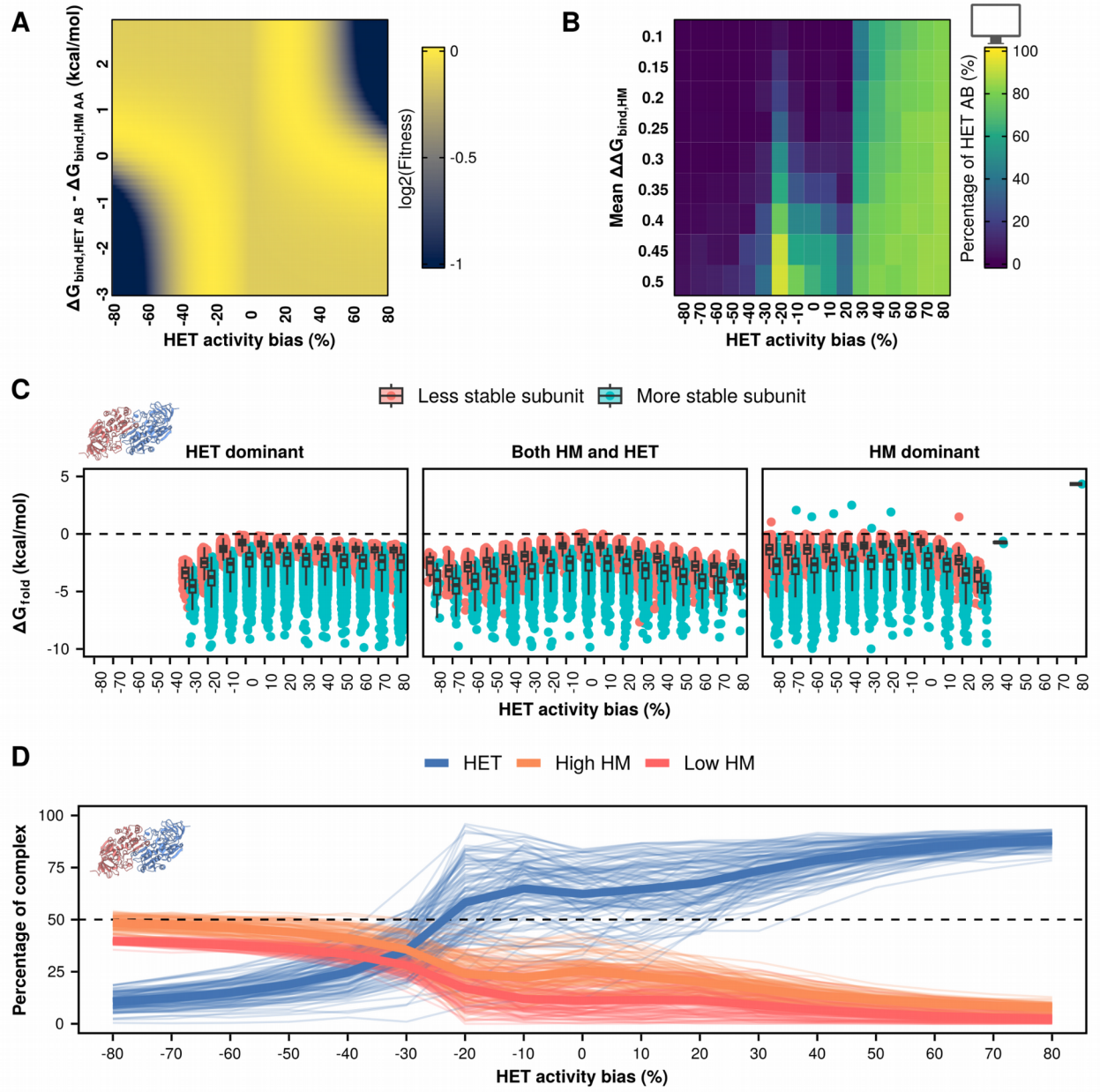

Figure S15. Simulations with differences in specific activity and lower optimal total activity (alpha = 60).

A. Fitness landscape when the optimal activity is set to 60. $\Delta\Delta G_{bind,AA}$, and $\Delta\Delta G_{bind,BB}$ remain constant throughout at -10 kcal/mol.

B. Percentages of heterodimers at the end of parametric simulations with different values of specific activity and varying mean effects of mutations on homodimers.

C. ΔG_{fold} values at the end of simulations with alpha = 60 and different specific activities for homo- and heterodimers. Disfavored outcomes, such as HET dominant when the heterodimer is less active, can still be reached if the subunits remain stable.

D. Percentages of heterodimers and each of the two homodimers for each of the 104 tested structures when simulations consider different specific activities of homo- and heterodimers. The two homodimers were distinguished based on their abundance.

47

1044 # References

1045 Abrusán G & Foguet C (2023) An Assessment of Quaternary Structure Functionality in
1046 Homomer Protein Complexes. *Mol Biol Evol* 40

1047 Adrain C & Freeman M (2012) New lives for old: evolution of pseudoenzyme function illustrated
1048 by iRhoms. *Nat Rev Mol Cell Biol* 13: 489–498

1049 Amoutzias GD, Robertson DL, Van de Peer Y & Oliver SG (2008) Choose your partners:
1050 dimerization in eukaryotic transcription factors. *Trends Biochem Sci* 33: 220–229

1051 André I, Strauss CEM, Kaplan DB, Bradley P & Baker D (2008) Emergence of symmetry in
1052 homooligomeric biological assemblies. *Proc Natl Acad Sci U S A* 105: 16148–16152

1053 Ashenberg O, Rozen-Gagnon K, Laub MT & Keating AE (2011) Determinants of
1054 Homodimerization Specificity in Histidine Kinases. *J Mol Biol* 413: 222–235

1055 Aubé S, Nielly-Thibault L & Landry CR (2023) Evolutionary trade-off and mutational bias could
1056 favor transcriptional over translational divergence within paralog pairs. *PLoS Genet* 19:
1057 e1010756

1058 Badonyi M & Marsh JA (2023) Buffering of genetic dominance by allele-specific protein complex
1059 assembly. *Sci Adv* 9: eadf9845

1060 Baker CR, Hanson-Smith V & Johnson AD (2013) Following gene duplication, paralog
1061 interference constrains transcriptional circuit evolution. *Science* 342: 104–108

1062 Bergendahl LT & Marsh JA (2017) Functional determinants of protein assembly into homomeric
1063 complexes. *Sci Rep* 7: 4932

1064 Berman HM, Westbrook J, Feng Z, Gilliland G, Bhat TN, Weissig H, Shindyalov IN & Bourne PE
1065 (2000) The Protein Data Bank. *Nucleic Acids Res* 28: 235–242

1066 Boncoeur E, Durmort C, Bernay B, Ebel C, Di Guilmi AM, Croizé J, Vernet T & Jault J-M (2012)
1067 PatA and PatB form a functional heterodimeric ABC multidrug efflux transporter responsible
1068 for the resistance of Streptococcus pneumoniae to fluoroquinolones. *Biochemistry* 51:
1069 7755–7765

1070 Brevet A, Chen J, Lévêque F, Blanquet S & Plateau P (1995) Comparison of the enzymatic
1071 properties of the two Escherichia coli lysyl-tRNA synthetase species. *J Biol Chem* 270:
1072 14439–14444

1073 Bridgham JT, Brown JE, Rodríguez-Marí A, Catchen JM & Thornton JW (2008) Evolution of a
1074 new function by degenerative mutation in cephalochordate steroid receptors. *PLoS Genet*
1075 4: e1000191

1076 Cano AV, Rozhoňová H, Stoltzfus A, McCandlish DM & Payne JL (2022) Mutation bias shapes
1077 the spectrum of adaptive substitutions. *Proc Natl Acad Sci U S A* 119

1078 Charlesworth B (2009) Fundamental concepts in genetics: effective population size and patterns
1079 of molecular evolution and variation. *Nat Rev Genet* 10: 195–205

1080 Cheng H, Schaeffer RD, Liao Y, Kinch LN, Pei J, Shi S, Kim B-H & Grishin NV (2014) ECOD: an
1081 evolutionary classification of protein domains. *PLoS Comput Biol* 10: e1003926

1082 Choi J-M, Serohijos AWR, Murphy S, Lucarelli D, Lofranco LL, Feldman A & Shakhnovich EI
1083 (2015) Minimalistic predictor of protein binding energy: contribution of solvation factor to
1084 protein binding. *Biophys J* 108: 795–798

1085 Conant GC & Wolfe KH (2008) Turning a hobby into a job: how duplicated genes find new
1086 functions. *Nat Rev Genet* 9: 938–950

1087 Dandage R & Landry CR (2019) Paralog dependency indirectly affects the robustness of human
1088 cells. *Mol Syst Biol* 15: e8871

1089 Delgado J, Radusky LG, Cianferoni D & Serrano L (2019) FoldX 5.0: working with RNA, small
1090 molecules and a new graphical interface. *Bioinformatics* 35: 4168–4169

1091 Deng C, Cheng C-HC, Ye H, He X & Chen L (2010) Evolution of an antifreeze protein by
1092 neofunctionalization under escape from adaptive conflict. *Proc Natl Acad Sci U S A* 107:
1093 21593–21598

1094 Dey S, Ritchie DW & Levy ED (2018) PDB-wide identification of biological assemblies from
1095 conserved quaternary structure geometry. *Nat Methods* 15: 67–72

1096 Diss G, Gagnon-Arsenault I, Dion-Coté A-M, Vignaud H, Ascencio DI, Berger CM & Landry CR
1097 (2017) Gene duplication can impart fragility, not robustness, in the yeast protein interaction
1098 network. *Science* 355: 630–634

1099 Ebert MCCJC, Maximilian C C J, Morley KL, Volpato JP, Schmitzer AR & Pelletier JN (2015)
1100 Asymmetric mutations in the tetrameric R67 dihydrofolate reductase reveal high tolerance
1101 to active-site substitutions. *Protein Sci* 24: 495–507

1102 Emlaw JR, Tessier CJG, McCluskey GD, McNulty MS, Sheikh Y, Burkett KM, Musgaard M &
1103 daCosta CJB (2021) A single historical substitution drives an increase in acetylcholine
1104 receptor complexity. *Proc Natl Acad Sci U S A* 118

1105 Finnigan GC, Hanson-Smith V, Stevens TH & Thornton JW (2012) Evolution of increased
1106 complexity in a molecular machine. *Nature* 481: 360–364

1107 Force A, Lynch M, Pickett FB, Amores A, Yan YL & Postlethwait J (1999) Preservation of
1108 duplicate genes by complementary, degenerative mutations. *Genetics* 151: 1531–1545

1109 Fu L, Niu B, Zhu Z, Wu S & Li W (2012) CD-HIT: accelerated for clustering the next-generation
1110 sequencing data. *Bioinformatics* 28: 3150–3152

1111 Garcia-Seisdedos H, Empereur-Mot C, Elad N & Levy ED (2017) Proteins evolve on the edge of
1112 supramolecular self-assembly. *Nature* 548: 244–247

1113 Gibson TA & Goldberg DS (2009) Questioning the ubiquity of neofunctionalization. *PLoS*
1114 *Comput Biol* 5: e1000252

1115 Gout J-F, Kahn D, Duret L & Paramecium Post-Genomics Consortium (2010) The relationship
1116 among gene expression, the evolution of gene dosage, and the rate of protein evolution.
1117 *PLoS Genet* 6: e1000944

1118 Gout J-F & Lynch M (2015) Maintenance and Loss of Duplicated Genes by Dosage
1119 Subfunctionalization. *Mol Biol Evol* 32: 2141–2148

1120 Hausser J, Mayo A, Keren L & Alon U (2019) Central dogma rates and the trade-off between
1121 precision and economy in gene expression. *Nat Commun* 10: 68

1122 Hernández-Hernández T, Martínez-Castilla LP & Alvarez-Buylla ER (2007) Functional
1123 diversification of B MADS-box homeotic regulators of flower development: Adaptive
1124 evolution in protein-protein interaction domains after major gene duplication events. *Mol*
1125 *Biol Evol* 24: 465–481

1126 He X & Zhang J (2005) Rapid subfunctionalization accompanied by prolonged and substantial
1127 neofunctionalization in duplicate gene evolution. *Genetics* 169: 1157–1164

1128 Hochberg GKA, Liu Y, Marklund EG, Metzger BPH, Laganowsky A & Thornton JW (2020) A
1129 hydrophobic ratchet entrenches molecular complexes. *Nature* 588: 503–508

1130 Hochberg GKA, Shepherd DA, Marklund EG, Santhanagoplan I, Degiacomi MT, Laganowsky A,
1131 Allison TM, Basha E, Marty MT, Galpin MR, *et al* (2018) Structural principles that enable
1132 oligomeric small heat-shock protein paralogs to evolve distinct functions. *Science* 359:
1133 930–935

1134 Jankauskaitė J, Jiménez-García B, Dapkūnas J, Fernández-Recio J & Moal IH (2018) SKEMPI
1135 2.0: an updated benchmark of changes in protein–protein binding energy, kinetics and
1136 thermodynamics upon mutation. *Bioinformatics* 35: 462–469

1137 Johri P, Gout J-F, Doak TG & Lynch M (2022) A Population-Genetic Lens into the Process of
1138 Gene Loss Following Whole-Genome Duplication. *Mol Biol Evol* 39

1139 Kabsch W & Sander C (1983) Dictionary of protein secondary structure: pattern recognition of
1140 hydrogen-bonded and geometrical features. *Biopolymers* 22: 2577–2637

1141 Kafková L, Debler EW, Fisk JC, Jain K, Clarke SG & Read LK (2017) The Major Protein
1142 Arginine Methyltransferase in Trypanosoma brucei Functions as an Enzyme-Prozyme
1143 Complex. *J Biol Chem* 292: 2089–2100

1144 Kemble H, Eisenhauer C, Couce A, Chapron A, Magnan M, Gautier G, Le Nagard H, Nghe P &
1145 Tenaillon O (2020) Flux, toxicity, and expression costs generate complex genetic
1146 interactions in a metabolic pathway. *Sci Adv* 6: eabb2236

1147 Kidd RD, Baker HM, Mathews AJ, Brittain T & Baker EN (2001) Oligomerization and ligand
1148 binding in a homotetrameric hemoglobin: two high-resolution crystal structures of
1149 hemoglobin Bart's (gamma(4)), a marker for alpha-thalassemia. *Protein Sci* 10: 1739–1749

1150 Kurtz A, Rollema HS & Bauer C (1981) Heterotropic interactions in monomeric βSH chains from
1151 human hemoglobin. *Arch Biochem Biophys* 210: 200–203

1152 Kuzmin E, Taylor JS & Boone C (2022) Retention of duplicated genes in evolution. *Trends*
1153 *Genet* 38: 59–72

1154 Levy ED & Teichmann S (2013) Structural, evolutionary, and assembly principles of protein
1155 oligomerization. In *Progress in Molecular Biology and Translational Science*, Giraldo J &
1156 Ciruela F (eds) pp 25–51. Academic Press

1157 Li W & Godzik A (2006) Cd-hit: a fast program for clustering and comparing large sets of protein
1158 or nucleotide sequences. *Bioinformatics* 22: 1658–1659

1159 Li Y, Zhang R, Wang C, Forouhar F, Clarke OB, Vorobiev S, Singh S, Montelione GT, Szyperski
1160 T, Xu Y, *et al* (2022) Oligomeric interactions maintain active-site structure in a
1161 noncooperative enzyme family. *EMBO J* 41: e108368

1162 Lukatsky DB, Shakhnovich BE, Mintseris J & Shakhnovich EI (2007) Structural similarity
1163 enhances interaction propensity of proteins. *J Mol Biol* 365: 1596–1606

1164 Lynch M (2006) Streamlining and simplification of microbial genome architecture. *Annu Rev*
1165 *Microbiol* 60: 327–349

1166 Lynch M (2007) The frailty of adaptive hypotheses for the origins of organismal complexity. *Proc*
1167 *Natl Acad Sci U S A* 104 Suppl 1: 8597–8604

1168 Lynch M (2012) The evolution of multimeric protein assemblages. *Mol Biol Evol* 29: 1353–1366

1169 Lynch M (2013) Evolutionary diversification of the multimeric states of proteins. *Proc Natl Acad*
1170 *Sci U S A* 110: E2821–8

1171 Lynch M & Conery JS (2000) The evolutionary fate and consequences of duplicate genes.
1172 *Science* 290: 1151–1155

1173 Lynch M & Force A (2000) The probability of duplicate gene preservation by
1174 subfunctionalization. *Genetics* 154: 459–473

1175 Mallik S & Tawfik DS (2020) Determining the interaction status and evolutionary fate of
1176 duplicated homomeric proteins. *PLoS Comput Biol* 16: e1008145

1177 Mallik S, Tawfik DS & Levy ED (2022) How gene duplication diversifies the landscape of protein
1178 oligomeric state and function. *Curr Opin Genet Dev* 76: 101966

1179 Mamnun YM, Pandjaitan R, Mahé Y, Delahodde A & Kuchler K (2002) The yeast zinc finger
1180 regulators Pdr1p and Pdr3p control pleiotropic drug resistance (PDR) as homo- and
1181 heterodimers in vivo. *Mol Microbiol* 46: 1429–1440

1182 Marchant A, Cisneros AF, Dubé AK, Gagnon-Arsenault I, Ascencio D, Jain H, Aubé S, Eberlein
1183 C, Evans-Yamamoto D, Yachie N, *et al* (2019) The role of structural pleiotropy and
1184 regulatory evolution in the retention of heteromers of paralogs. *eLife* 8: e46754

1185 Metzger BPH, Duveau F, Yuan DC, Tryban S, Yang B & Wittkopp PJ (2016) Contrasting
1186 Frequencies and Effects of cis- and trans-Regulatory Mutations Affecting Gene Expression.
1187 *Mol Biol Evol* 33: 1131–1146

1188 Muñoz-Gómez SA, Bilolikar G, Wideman JG & Geiler-Samerotte K (2021) Constructive Neutral
1189 Evolution 20 Years Later. *J Mol Evol* 89: 172–182

1190 Oughtred R, Rust J, Chang C, Breitkreutz B-J, Stark C, Willems A, Boucher L, Leung G, Kolas
1191 N, Zhang F, *et al* (2021) The BioGRID database: A comprehensive biomedical resource of
1192 curated protein, genetic, and chemical interactions. *Protein Sci* 30: 187–200

1193 Pace CN (1975) The stability of globular proteins. *CRC Crit Rev Biochem* 3: 1–43

1194 Pareek G, Samaddar M & D'Silva P (2011) Primary sequence that determines the functional
1195 overlap between mitochondrial heat shock protein 70 Ssc1 and Ssc3 of Saccharomyces
1196 cerevisiae. *J Biol Chem* 286: 19001–19013

1197 Paul MD & Hristova K (2019) The RTK Interactome: Overview and Perspective on RTK
1198 Heterointeractions. *ACS Chem Rev* 119: 5881–5921

1199 Pereira-Leal JB, Levy ED, Kamp C & Teichmann SA (2007) Evolution of protein complexes by
1200 duplication of homomeric interactions. *Genome Biol* 8: R51

1201 Pettersen EF, Goddard TD, Huang CC, Meng EC, Couch GS, Croll TI, Morris JH & Ferrin TE
1202 (2021) UCSF ChimeraX: Structure visualization for researchers, educators, and
1203 developers. *Protein Sci* 30: 70–82

1204 Pillai AS, Chandler SA, Liu Y, Signore AV, Cortez-Romero CR, Benesch JLP, Laganowsky A,
1205 Storz JF, Hochberg GKA & Thornton JW (2020) Origin of complexity in haemoglobin
1206 evolution. *Nature* 581: 480–485

1207 Pils B & Schultz J (2004) Inactive enzyme-homologues find new function in regulatory
1208 processes. *J Mol Biol* 340: 399–404

1209 Plaxco KW, Simons KT, Ruczinski I & Baker D (2000) Topology, stability, sequence, and length:
1210 defining the determinants of two-state protein folding kinetics. *Biochemistry* 39: 11177–
1211 11183

1212 Roos D & de Boer M (2021) Mutations in cis that affect mRNA synthesis, processing and
1213 translation. *Biochim Biophys Acta Mol Basis Dis* 1867: 166166

1214 Rotem A, Serohijos AWR, Chang CB, Wolfe JT, Fischer AE, Mehoke TS, Zhang H, Tao Y, Lloyd
1215 Ung W, Choi J-M, *et al* (2018) Evolution on the Biophysical Fitness Landscape of an RNA
1216 Virus. *Mol Biol Evol* 35: 2390–2400

1217 Sailer ZR & Harms MJ (2017) Molecular ensembles make evolution unpredictable. *Proc Natl*
1218 *Acad Sci U S A* 114: 11938–11943

1219 Schulz L, Sendker FL & Hochberg GKA (2022) Non-adaptive complexity and biochemical
1220 function. *Curr Opin Struct Biol* 73: 102339

1221 Schweke H, Levin T, Pacesa M, Goverde CA, Kumar P, Duhoo Y, Dornfeld LJ, Dubreuil B,
1222 Georgeon S, Ovchinnikov S, *et al* (2023) An atlas of protein homo-oligomerization across
1223 domains of life. *bioRxiv*: 2023.06.09.544317

1224 Shiber A, Döring K, Friedrich U, Klann K, Merker D, Zedan M, Tippmann F, Kramer G & Bukau B
1225 (2018) Cotranslational assembly of protein complexes in eukaryotes revealed by ribosome
1226 profiling. *Nature* 561: 268–272

1227 Stoltzfus A (1999) On the possibility of constructive neutral evolution. *J Mol Evol* 49: 169–181

1228 Stutz C & Blein S (2020) A single mutation increases heavy-chain heterodimer assembly of
1229 bispecific antibodies by inducing structural disorder in one homodimer species. *J Biol*
1230 *Chem* 295: 9392–9408

1231 Svensson EI & Berger D (2019) The Role of Mutation Bias in Adaptive Evolution. *Trends Ecol*

Evol 34: 422–434

Tiberti M, Terkelsen T, Degn K, Beltrame L, Cremers TC, da Piedade I, Di Marco M, Maiani E & Papaleo E (2022) MutateX: an automated pipeline for in silico saturation mutagenesis of protein structures and structural ensembles. *Brief Bioinform* 23: bbac074

Tsai CJ, Lin SL, Wolfson HJ & Nussinov R (1996) Protein-protein interfaces: architectures and interactions in protein-protein interfaces and in protein cores. Their similarities and differences. *Crit Rev Biochem Mol Biol* 31: 127–152

Usmanova DR, Bogatyreva NS, Bernad JA, Eremina AA, Gorshkova AA, Kanevskiy GM, Lonishin LR, Meister AV, Yakupova AG, Kondrashov FA, *et al* (2018) Self-consistency test reveals systematic bias in programs for prediction change of stability upon mutation. *Bioinformatics* 34: 3653–3658

Verma M, Choi J, Cottrell KA, Lavagnino Z, Thomas EN, Pavlovic-Djuranovic S, Szczesny P, Piston DW, Zaher HS, Puglisi JD, *et al* (2019) A short translational ramp determines the efficiency of protein synthesis. *Nat Commun* 10: 5774

Wang Z, Stalcup LD, Harvey BJ, Weber J, Chloupkova M, Dumont ME, Dean M & Urbatsch IL (2006) Purification and ATP hydrolysis of the putative cholesterol transporters ABCG5 and ABCG8. *Biochemistry* 45: 9929–9939

Wilke CO, Wang JL, Ofria C, Lenski RE & Adami C (2001) Evolution of digital organisms at high mutation rates leads to survival of the flattest. *Nature* 412: 331–333

Young RS, Hayashizaki Y, Andersson R, Sandelin A, Kawaji H, Itoh M, Lassmann T, Carninci P, FANTOM Consortium, Bickmore WA, *et al* (2015) The frequent evolutionary birth and death of functional promoters in mouse and human. *Genome Res* 25: 1546–1557

Young RS, Talmane L, Marion de Procé S & Taylor MS (2022) The contribution of evolutionarily volatile promoters to molecular phenotypes and human trait variation. *Genome Biol* 23: 89

53